Search for Ξ^* production in K^-p interactions at 2.87 GeV/c †

E. Briefel,‡ S. A. Gourevitch,§ L. Kirsch, and P. Schmidt
Brandeis University, Waltham, Massachusetts 02154

C. Y. Chang, R. J. Hemingway,‖ B. V. Khoury, A. R. Stottlemyer,¶ and G. B. Yodh
University of Maryland, College Park, Maryland 20742

R. C. Fernow,** S. L. Glickman,†† M. Goldberg, S. M. Jacobs,†† B. T. Meadows,‡‡ G. C. Moneti, and D. P. Weygand
Syracuse University, Syracuse, New York 13210

J. Tompkins, J. Canter, E. Katsoufis,§§ W. A. Mann, J. Schneps, and G. Wolsky¶¶
Tufts University, Medford, Massachusetts 02155

(Received 11 January 1977; revised manuscript received 3 June 1977)

Evidence is presented for production of Ξ^* resonances, decaying into $\Xi\pi$, $\Xi(1530)\pi$, $\Lambda\bar{K}$, and $\Sigma\bar{K}$, in K^-p interactions at 2.87 GeV/c. The data represent final combined results from a 30-events/μb hydrogen exposure and an 18-events/μb exposure in deuterium designed to study Ξ^* production in the mass interval 1.46–2.07 GeV/c^2. In addition to $\Xi(1820)$ and $\Xi(1940)$, signals have been observed at masses of 1630 MeV/c^2 and 1860 MeV/c^2 decaying into $\Xi^-\pi^+$ and $Y\bar{K}$, respectively. Reaction cross sections have been measured for all final states containing two visible signs of strangeness, and for the final states ΛK^-K^+ and $\Sigma^0K^-K^+$.

I. INTRODUCTION

A search has been completed for evidence of Ξ resonances in the mass range 1.5–2.0 GeV/c^2 decaying into $\Xi\pi$, $\Xi\pi\pi$, $\Xi(1530)\pi$, $Y\bar{K}$, and $Y\bar{K}\pi$. We are reporting the combined results of two experiments involving K^-p interactions at 2.87 GeV/c, one using a hydrogen target and the other a deuterium target. The results of a search for Ξ^* production in K^-n interactions, which was the primary purpose of the deuterium experiment, have been reported previously.[1] Partial results on the reactions

$$K^-p \to \Xi^*K\,, \quad \Xi^* \to \Xi\pi(\pi) \tag{1}$$

in hydrogen have also been published.[2] The present paper contains our final results for the $\Xi\pi K(\pi)$ final states of reaction (1), as well as for $Y\bar{K}K(\pi)$ final states, utilizing both the hydrogen data and K^-p interactions extracted from the deuterium data.

The reactions of interest here are

$$K^-p \to \Xi^-\pi^+K^0 \tag{2}$$
$$\to \Xi^-\pi^0K^+ \tag{3}$$
$$\to \Xi^-\pi^+\pi^0K^0 \tag{4}$$
$$\to \Xi^-\pi^-\pi^+K^+ \tag{5}$$
$$\to \Xi^0\pi^-\pi^+K^0 \tag{6}$$
$$\to \Lambda\bar{K}^0K^0 \tag{7}$$
$$\to \Lambda\bar{K}\pi K \tag{8}$$
$$\to \Sigma^-\bar{K}^0K^+ \tag{9}$$
$$\to \Sigma^+K^-K^0 \tag{10}$$
$$\to \Sigma\bar{K}\pi K \tag{11}$$
$$\to \Lambda K^-K^+ \tag{12}$$
$$\to \Sigma^0K^-K^+ \tag{13}$$
$$\to \Xi^0\pi^-K^+\,. \tag{14}$$

The events of reactions (2)–(11) were required to exhibit two visible signs of strangeness in the form of neutral or charged decays, and have been obtained from both the hydrogen exposure (with a sensitivity of 30 events/μb) and the deuterium exposure (with a sensitivity of 18 events/μb). The events of reactions (12)–(14) resulted from a separate scan of a portion of the hydrogen film (with a sensitivity of 23.1 events/μb) for topologies involving two charged prongs and a neutral V^0 from production. The details of the experimental procedure and event selection criteria will be given in Secs. II and III. Cross sections have been measured for reactions (2)–(13) and are presented in Sec. IV.

The paucity of information on Ξ states is well known, and can be attributed to the experimental difficulties (principally low cross sections) associated with the study of strangeness-(–2) final states. Because of the low statistics available in such studies, the usual criterion of about five-standard-deviations significance for resonance candidates has generally been relaxed to about

three for Ξ^* signals. In addition to the well-established $\Xi(1530)$, previous experiments[3] have indicated, at or above the reduced standard of significance, the presence of Ξ states at masses of 1820 and 1940 MeV/c^2. The $\Xi(1820)$ has been observed to decay into $Y\overline{K}$, $\Xi\pi$, $\Xi\pi\pi$, and $\Xi(1530)\pi$; $\Xi(1940)$ has only been observed in $\Xi\pi$ and $\Xi(1530)\pi$ mass combinations. The masses and primary decay modes of these resonances are roughly compatible with recent SU(3)-multiplet assignments.[4] In addition, a possible $\Xi(1630)$ has received some attention.[2,5] Although it does not fit within the SU(3) assignments of Ref. 4, it does have a place in the SU(6) × O(3) symmetry scheme.[6]

Our evidence for the possible production of Ξ resonances in the final-state mass distributions of reactions (2)–(14) will be presented in Sec. V. A summary of our results can be found in Sec. VI.

II. EXPERIMENTAL DETAILS

The data for this analysis came from two separate exposures, consisting of ~10^6 pictures each, of the BNL 31-in. bubble chamber to a separated beam of 2.87-GeV/c K^- mesons. During the first exposure the chamber was filled with hydrogen at a density of 0.060 ± 0.001 g/cm^3. The second exposure, which consisted of six separate runs, was taken with the chamber filled with deuterium[7] at an average density of 0.131 g/cm^3. Beam content for the hydrogen exposure was determined by a count of the total numbers of interactions and one-prong decays of K^- in a subsample of the film. Percentages of K^-, π^-, and μ^- were measured to be $(84 \pm 3)\%$, $(8.2 \pm 2.9)\%$, and $(7.9 \pm 3.4)\%$, respectively. The K^- content of the beam for the deuterium exposure was determined by analysis of $K^- \to \pi^-\pi^-\pi^+$ decays, and found to vary considerably over the separate runs, with an average value of $(76 \pm 4)\%$. No information on the relative π^- and μ^- contamination is available for the deuterium experiment.

Using a fiducial volume of length 64.0 cm in the beam direction, the total proton target sensitivities of the hydrogen and deuterium exposures amount to 30 ± 1 and 18.0 ± 0.5 events/μb, respectively. For the purpose of cross-section calculations a subsample of the deuterium exposure corresponding to 15.8 ± 0.4 events/μb has been used. The scan for events with the two-prong–plus-V^0 topology [from which reactions (12)–(14) are obtained] was carried out in a subsample of the hydrogen exposure amounting to 23.1 ± 0.8 events/μb.

All the film was scanned twice in all three views for events with two or more visible signs of strangeness.[8] Approximately two thirds of the hydrogen film was then scanned for events with two charged prongs and one decaying V^0. All candidates were measured on either film-plane or image-plane digitizing machines and processed through the geometry and kinematics programs TVGP and SQUAW. Consistency of observed and computed ionizations of charged tracks was checked by physicists for all events passing the reconstruction process. Wherever possible, ionization criteria were used to resolve kinematic ambiguities. Poorly measured events, and events failing to fit an acceptable hypothesis, were reprocessed at least once.

The fitting and selection of K^-p interactions among the deuterium events requires special comment. Final states containing no missing neutrals other than a neutron from the deuteron can be fitted with one constraint at the production vertex. To select K^-p interactions we require the momentum of the neutron to be less than 200 MeV/c. The spectator-neutron momentum distribution for such events is shown in Fig. 1. The agreement with the distribution expected on the basis of the Hamada-Johnston[9] deuteron wave function is not as good as that observed for spectator protons from K^-n interactions.[1] This is due to the poorer resolution in the momentum of the unseen neutron. The solid curve in Fig. 1 represents the normalized Hamada-Johnston distribution after integration with the spectator-neutron resolution function. It is in adequate agreement with the observed spectrum.

On the other hand final states which contain missing neutrals as well as the spectator neutron, such as $K^-d \to \Lambda_1 K_1^0 K_2^0 n_s$,[10] are underconstrained at the production vertex. Such events have been fitted by ignoring the neutron and assuming a stationary proton target. Since this procedure may introduce a substantial and unknown processing in-

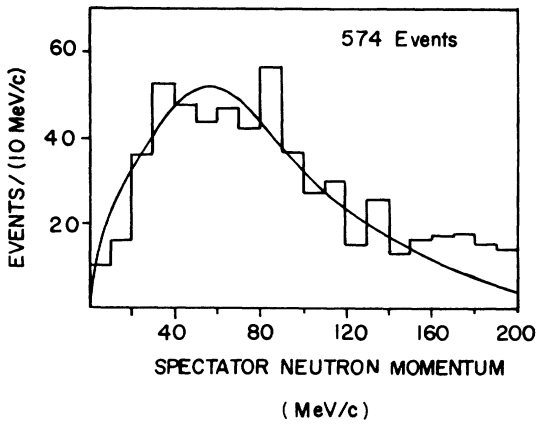

FIG. 1. Spectator-neutron momentum distribution for final states in which all reaction products are measured. Solid curve is the normalized Hamada-Johnston distribution modified by the neutron momentum resolution function.

efficiency, these channels cannot be used for cross-section calculations. We expect, however, that those deuterium events successfully fit by this procedure will involve relatively low-momentum nucleons. Final-state mass distributions, therefore, should be minimally affected by inclusion of these events. Further checks on this procedure will be discussed in Sec. V.

The scan for events with at least two visible signs of strangeness in the hydrogen exposure yielded a total of 3510 events, of which 3020 yielded a fit to a constrained final state. The corresponding scan in deuterium yielded 4811 events (K^-n plus K^-p), of which 1850 either had a constrained production vertex fit with a neutron momentum <200 MeV/c, or a fit to a K^-p reaction with an assumed stationary proton target. The two-prong-plus-V^0 scan in hydrogen produced 58 229 events, with approximately 1800 events involving reactions (12)–(14).

III. AMBIGUITY RESOLUTION

The kinematic ambiguity level for events with two visible signs of strangeness (~8%) is an order of magnitude less than that for events of the two-prong-plus-V^0 topology [80% for the events of reactions (12)–(14)]. We therefore discuss the two cases separately.

The major ambiguities in the former sample occur between the following reactions:

$$K^-p \to \Xi_1^-\pi^+K_2^0 \text{ vs } K^-p \to \Xi_1^-\pi^0K^+ \tag{15}$$

and

$$K^-p \to \Lambda_1 K_1^0 K_2^0 \tag{16a}$$

vs

$$\pi^-p \to \Lambda_1 K_1^0\pi^0 . \tag{16b}$$

(The subscripts 1 and 2 have been defined in Ref. 10.) The $\pi^+K_2^0, \pi^0K^+$ ambiguity of reactions (15) involves 140 events and is essentially unresolvable. The events have been assigned to each of the two final states with a weight of $\frac{1}{2}$. There are 75 events ambiguous between reactions (16). Attempts to fit hypothesis (16b) were made on 60% of the events exhibiting two visible decays of neutral strange particles and no charged prongs from production. On the basis of our beam composition, the cross section for reaction (16b),[11] and visibility and efficiency factors, we would expect 37 ± 17 such events in our final sample. We observe 21 events uniquely fitting reaction (16b), consistent with expectations within one standard deviation. Moreover, the fit probability distribution for hypothesis (16a) is uniform for the ambiguous events, whereas the same distribution for these events interpreted as reaction (16b) is distinctly nonuniform (53% of the events having probability less than 10%). Finally, the $M(K_1^0K_2^0)$ spectrum for the ambiguous reaction (16a) events exhibits the characteristic $\phi(1019)$ peak, and is consistent with the distribution obtained for unique $K^-p \to \Lambda_1 K_1^0 K_2^0$ events. For these reasons we have assigned all the ambiguous events to the reaction (16a).

An additional 100 events, distributed among various reaction channels, involve ambiguities of the following types:

(i) Λ_1 versus K_1^0 unresolved by ionization,

(ii) Σ^- versus Ξ_2^-, and

(iii) a four-constraint (4C) fit versus a one-constraint (1C) fit with a π^0.

When true Λ's fit the K^0 hypothesis, we expect the V^0 center-of-mass decay angular distribution $\hat{\Lambda}\cdot\hat{p}$ to be uniform, and the distribution in $\hat{K}^0\cdot\hat{\pi}^+$ to be peaked forward. The events involving ambiguity (i) exhibit this behavior and have been assigned to the Λ hypothesis. A study of events involving the ambiguity (ii) in K^-n interactions[1] has shown an overwhelming preference for the Σ^- hypothesis. We have therefore made the same assignment here for the 15 ambiguous events. Finally, the ambiguities involving a choice between a 4C fit and a 1C fit have been decided in favor of the more highly constrained hypothesis.

The remaining unresolved ambiguities in the sample of events having two visible signs of strangeness, involving approximately 90 events, have been assigned equally to the competing hypotheses. With the exception of the reactions $K^-p \to \Lambda_1 K^-K_1^0\pi^+$ and $K^-p \to \Xi_1^0\pi^-\pi^+K_1^0$, the ambiguity rate in any channel discussed is less than 10%.

Table I contains an ambiguity map for the two-prong-plus-V^0 events of reactions (12)–(14). There are 47 events which have a Λ_1, K_1^0 decay ambiguity of the V^0. Here again, the distributions in $\hat{\Lambda}\cdot\hat{p}$ and $\hat{K}^0\cdot\hat{\pi}^+$ indicate the correctness of the Λ assignment.

The other ambiguities are principally among the three reactions themselves and with the one-constraint reactions

$$K^-p \to \Lambda_1\pi^-\pi^+X^0 \quad (X^0=\gamma,\pi^0,\eta) . \tag{17}$$

The results of the somewhat involved analysis of these ambiguities are shown in Table III. The rest of this section describes in detail the criteria and tests that justify our choices. The uninterested reader may skip to the next section.

The ambiguities between the 4C reaction (12) and the lesser-constrained reactions (13), (14), and (17) have been decided in favor of the more highly constrained fit. In order to discuss our justification for this choice with respect to reactions (14) and (17), and for later use in resolving

TABLE I. Ambiguity map for the final states ΛK^-K^+, $\Sigma^0K^-K^+$, and $\Xi^0\pi^-K^+$. Entries represent the number of events in the final state at the left which are ambiguous with the final state indicated at the top of the column. Events involving multiple ambiguities will contribute to more than one entry.

	ΛK^-K^+	$\Sigma^0K^-K^+$	$\Xi^0\pi^-K^+$	$\Lambda\pi^-\pi^+X^0$	$\Lambda K^-K^+\pi^0$	Total number of events
ΛK^-K^+	166	196	215	378	1	723
$\Sigma^0K^-K^+$	196	55	228	388	44	482
$\Xi^0\pi^-K^+$	215	228	366	723	23	1265

the ambiguities of the final state $\Sigma^0K^-K^+$, we treat all the reactions indicated in Table I generically as

$$K^-p \to m^-m^+\Lambda_1 X^0. \tag{18}$$

The final-state particles (m^-, m^+) will be (K^-, K^+), (π^-, K^+), or (π^-, π^+), respectively, for reactions (12) and (13), (14), and (17). The symbol X^0 represents zero for reaction (12), γ for reaction (13), π^0 for reaction (14), and γ, π^0, or η for reactions (17). We further define the three variables $X_{\pi\pi}$, $X_{\pi K}$, and X_{KK} in the following manner: Using measured momenta for m^-, m^+, Λ_1, and the K^- beam, $X_{\pi\pi}$, $X_{\pi K}$, and X_{KK} are the cosines of the angle between the Λ and the (ΛX^0) system, in the (ΛX^0) center of mass, when m^-m^+ are interpreted as $\pi^-\pi^+$, π^-K^+, and K^-K^+, respectively. Table II indicates the distributions in these variables expected[12] for true samples of reactions (13), (14), and (17). The distributions in $X_{\pi\pi}$ and $X_{\pi K}$ for true $\Lambda K^-K^+(\pi^0)$ events will be the same as those for the final state $\Sigma^0K^-K^+$, precluding their use for discrimination between these channels.

Figure 2 contains the distributions in $X_{\pi\pi}$, $X_{\pi K}$, and X_{KK} for unique ΛK^-K^+ and $\Xi^0\pi^-K^+$ final states, as well as for events involving ambiguities between reaction (12) and reactions (14) and (17). The distributions for the three ambiguous samples are all consistent with those for unique ΛK^-K^+ events, and none exhibit the sharp backward peaking in X_{KK} expected for true $\Xi^0\pi^-K^+$ or $\Lambda\pi^-\pi^+X^0$ events. Figure 3(b) shows the distribution in $M(K^-K^+)$, formed from measured variables, for the events ambiguous with ΛK^-K^+ and having $X_{KK} < -0.7$ where we expect the highest concentration of contaminants. The $\phi(1019)$ peak characteristic of unique events [Fig. 3(a)] is evident. Also, neither the restricted sample of events of Fig. 3(b) having $X_{KK} < -0.7$, nor the full sample of ambiguous events, show any evidence for $K^*(890)$ in $M(\pi^-K^+)$, $\rho(770)$ in $M(\pi^-\pi^+)$, $\omega(783)$ in $M(\pi^-\pi^+\pi^0)$, or Y^* in $M(\Lambda\pi)$. Finally, we have studied the π^0

TABLE II. Expected distributions for the variables $X_{\pi\pi}$, $X_{\pi K}$, and X_{KK} (see text for definitions), for the final states $\Sigma^0K^-K^+$, $\Xi^0\pi^-K^+$, and $\Lambda\pi^-\pi^+X^0$.

	$\Sigma^0K^-K^+$	$\Xi^0\pi^-K^+$	$\Lambda\pi^-\pi^+X^0$
$X_{\pi\pi}$	Very forward	Forward	Uniform
$X_{\pi K}$	Forward	Uniform	Backward
X_{KK}	Uniform	Backward	Very backward

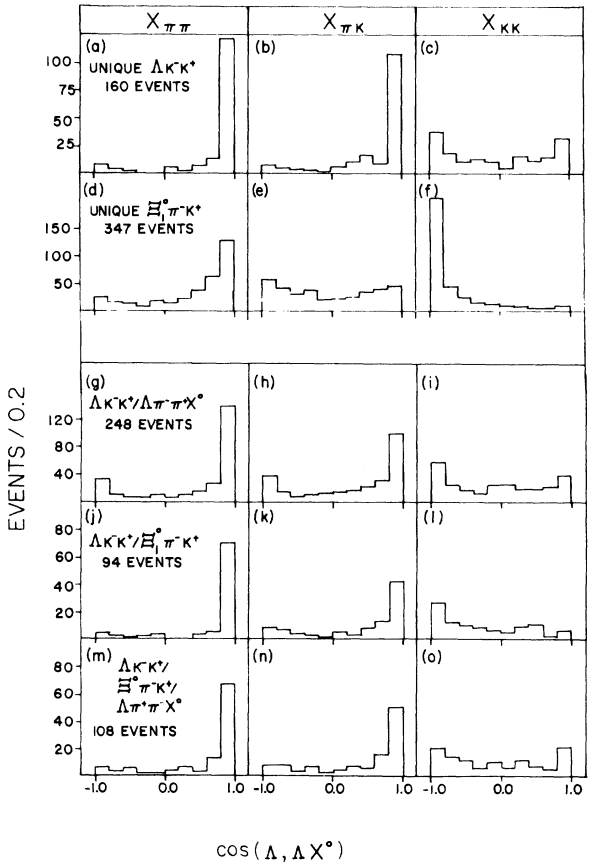

FIG. 2. Distributions in the measured variables $X_{\pi\pi}$, $X_{\pi K}$, and X_{KK} (see text for definitions). (a)–(c) Unique ΛK^-K^+ events. (d)–(f) Unique $\Xi^0\pi^-K^+$ events. (g)–(i) Events ambiguous between ΛK^-K^+ and $\Lambda\pi^-\pi^+X^0$. (j)–(l) Events ambiguous between ΛK^-K^+ and $\Xi^0\pi^-K^+$. (m)–(o) Events ambiguous among ΛK^-K^+ and $\Xi^0\pi^-K^+$ and $\Lambda\pi^-\pi^+X^0$.

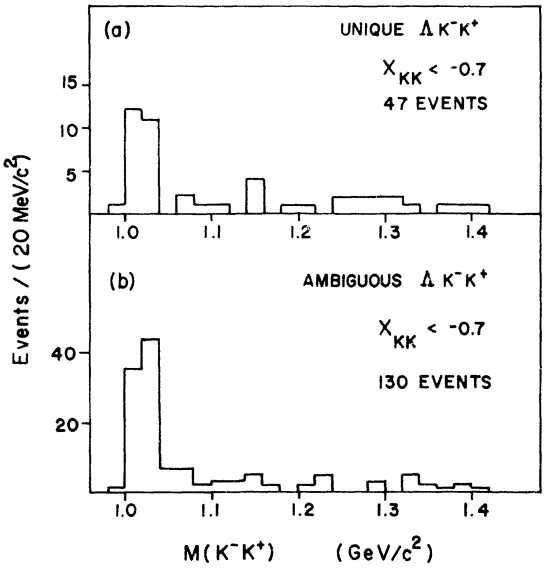

FIG. 3. Measured K^-K^+ effective mass for events having $X_{KK} < -0.7$ (see text). (a) Unique ΛK^-K^+ events. (b) Events ambiguous between the final state ΛK^-K^+ and the final states $\Xi^0\pi^-K^+$ and/or $\Lambda\pi^-\pi^+X^0$.

laboratory momentum spectra for the final state $\Lambda\pi^+\pi^-\pi^0$ with and without the events ambiguous with ΛK^-K^+. The π^0 momentum spectrum without the ambiguous events is smooth and consistent with the $\pi^\pm$ spectra, as expected. The addition of the ambiguous events creates a clear and sharp excess of low-momentum π^0's fully consistent with

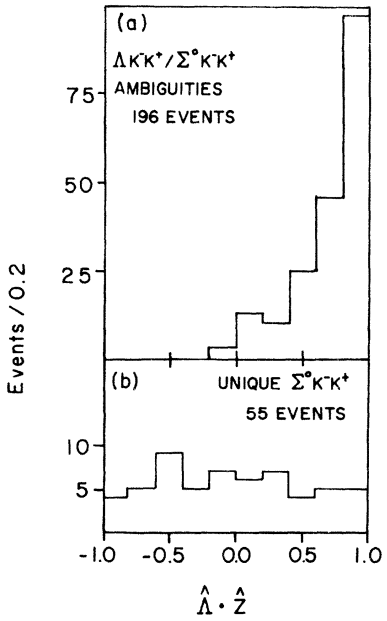

FIG. 4. Angular distribution $\hat{\Lambda}\cdot\hat{Z}$ (see text for definition of $\hat{Z}$). (a) Events ambiguous between the final states ΛK^-K^+ and $\Sigma^0K^-K^+$ (b) Unique $\Sigma^0K^-K^+$ events.

the ambiguous events *not* being $\Lambda\pi^+\pi^-\pi^0$. Our choice of reaction (12) therefore appears fully justified and we calculate, on the basis of the distributions in Fig. 3 and Fig. 2(f), an upper limit of 22 $\Xi^0\pi^-K^+$ and $\Lambda\pi^-\pi^+X^0$ events in the sample of events ambiguous with reaction (12), at the 90% confidence level.

The Λ-Σ^0_1 ambiguity between reactions (12) and (13) has been resolved on the basis of the distributions shown in Fig. 4. These represent the cosine of the angle between the Λ in the Σ^0 center-of-mass system, and the direction $\hat{Z}$ defined as

$$\hat{Z} = \frac{(\hat{K}^-_{\text{beam}} \times \hat{\Sigma}^0) \times \hat{\Sigma}^0}{|(\hat{K}^-_{\text{beam}} \times \hat{\Sigma}^0) \times \hat{\Sigma}^0|} . \tag{19}$$

The momenta used in (19) are in the laboratory frame, and fitted quantities are used throughout. The disparity between the ambiguous events of Fig. 4(a) and the unique $\Sigma^\circ K^-K^+$ events of Fig. 4(b) is evident. Using the number of ambiguous events having $\hat{\Lambda}\cdot\hat{Z} < 0$, we estimate an upper limit at the 90% confidence level of 12 $\Sigma^0K^-K^+$ events in the sample ambiguous with the final state ΛK^-K^+.

On the basis of the foregoing results we accept all 723 events fitting the highly constrained reaction (12) into the ΛK^-K^+ sample. At the 90% confidence level, the contamination from competing hypotheses does not exceed 5%.

In the sample of events fitting the final state $\Sigma^0K^-K^+$, there are 44 events ambiguous with the reaction $K^-p \to \Lambda K^-K^+\pi^0$. Studies of the missing-mass spectrum in K^-K^+(MM), and of the $\Sigma^0 \to \Lambda\gamma$ decay angle, have indicated the possibility that up to ~50% of these may indeed be Σ^0 events. However, since we have no clear means of separation, all 44 events have been excluded from the subsequent analysis, and the $\Sigma^0K^-K^+$ cross section has been adjusted to reflect this uncertainty. In Fig. 5 we show the distributions in $X_{\pi\pi}$, $X_{\pi K}$, and X_{KK} for unique $\Sigma^0K^-K^+$ events and for events sharing ambiguities between reactions (13), (14), and (17). The distributions for unique events [Figs. 5(a)–5(c)] are consistent with expectations except for some backward peaking in X_{KK}, which is contributed by the events having $X_{\pi\pi} < 0$. Also, the distributions for the ambiguous events [Figs. 5(d)–5(l)] indicate, with the exception of some backward peaking in Fig. 5(i), the validity of the Σ^0 hypothesis. In order to obtain a sample of reaction (13) events containing minimum contamination from reactions (14) and (17), we have only accepted events which satisfy the following conditions:

i. unique $\Sigma^0K^-K^+$ events, $X_{\pi\pi} > 0$;

ii. $\Sigma^0K^-K^+$ events ambiguous with $\Xi^0\pi^-K^+$, $X_{KK} > -0.7$; and

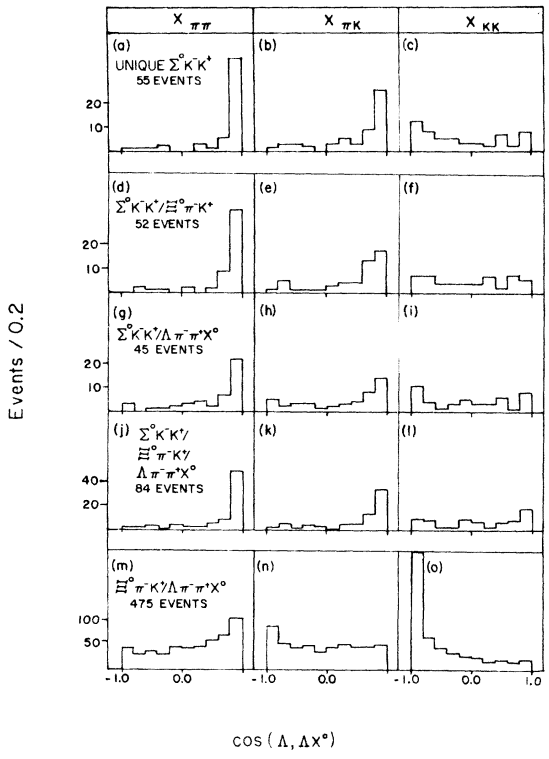

FIG. 5. Distribution in the measured variables $X_{\pi\pi}$, $X_{\pi K}$, and X_{KK} (see text for definitions). (a)–(c) Unique $\Sigma^0K^-K^+$ events. (d)–(f) Events ambiguous between $\Sigma^0K^-K^+$ and $\Xi^0\pi^-K^+$. (g)–(i) Events ambiguous between $\Sigma^0K^-K^+$ and $\Lambda\pi^-\pi^+X^0$. (j)–(l) Events ambiguous among $\Sigma^0K^-K^+$ and $\Xi^0\pi^-K^+$ and $\Lambda\pi^-\pi^+X^0$. (m)–(o) Events ambiguous between $\Xi^0\pi^-K^+$ and $\Lambda\pi^-\pi^+X^0$.

iii. $\Sigma^0K^-K^+$ events ambiguous with $\Lambda\pi^-\pi^+X^0$, $X_{\pi K}>0$ or $X_{KK}>-0.7$.

A total of 39 events are removed from the distributions of Figs. 5(c), 5(f), 5(i), 5(l) by these selections. This method yields a sample of 197 $K^-p \to \Sigma^0K^-K^+$ events which, on the basis of the distributions for the ambiguous events [Figs. 5(f), 5(h), 5(i), 5(k), 5(l)], unique $\Sigma^0K^-K^+$ events [Figs. 5(b), 5(c)] and unique $\Xi^0\pi^-K^+$ events [Figs. 2(e), 2(f)] contains, at the 90% confidence level, no more than 13 events belonging to reaction (14) or (17).

As can be seen from Table II, separation of events belonging to the Ξ^0 hypothesis of reaction (14) is not as readily available as was the case for the channels thus far discussed. Figures 5(m)–5(o) indicate that the ambiguous events contain substantial contamination by events belonging to the one-constraint reaction (17). We have found no reliable method of extracting the true $\Xi^0\pi^-K^+$ events from this sample, and exclude them from further consideration. Figures 2(d)–2(f) contain the relevant angular distributions for events uniquely fitting the Ξ^0 hypothesis. Examination of the two-dimensional plot of $X_{\pi\pi}$ versus $X_{\pi K}$ for these events indicates that there is an excess of events in the forward region of the $X_{\pi K}$ distribution contributed primarily by events in the very forward region of $X_{\pi\pi}$ ($X_{\pi\pi}>0.98$), consistent with the distributions for unique $\Sigma^0K^-K^+$ events. Similarly, the distribution in X_{KK} for events having $X_{\pi K}<-0.6$ shows a very sharp backward peak having $X_{KK}<-0.98$, consistent with that expected for the $\Lambda\pi^-\pi^+X^0$ final states. In order to obtain a sample of $\Xi^0\pi^-K^+$ events which contains a minimum contamination by events belonging to reactions (13) and (17), we have therefore only accepted events which uniquely fit this hypothesis and in addition have excluded those which satisfy the following two conditions:

$$X_{\pi\pi}\geq 0.98 \text{ if } X_{\pi K}\geq 0.70$$

or

$$X_{KK}\leq -0.99 \text{ if } X_{\pi K}\leq -0.60.$$

Based upon the distributions of Figs. 2(d)–2(f), 5(a)–5(c), the corresponding two-dimensional plots, and the distribution $M(K^-K^+)$ formed by using measured quantities and interpreting the π^- as a K^-, our final sample of 295 $\Xi^0\pi^-K^+$ events contains, at the 90% confidence level, less than 16% contamination by the final states $\Sigma^0K^-K^+$ and $\Lambda\pi^-\pi^+X^0$.

For convenience the results of the two-prong-plus-V^0 ambiguity resolution are summarized in Table III. The same analysis was carried out excluding events involving production of $\phi(1019)$. The assignment of the ambiguous events and the estimates of contamination remain unchanged.

TABLE III. Resolution of kinematic ambiguities in the final states ΛK^-K^+, $\Sigma^0K^-K^+$, and $\Xi^0\pi^-K^+$.

Final state	Unique events	Resolved ambiguities	Final sample	Estimated contamination
ΛK^-K^+	166	557	723	<5%
$\Sigma^0K^-K^+$	55	142	197	<7%
$\Xi^0\pi^-K^+$	366	0	295	<16%

IV. CROSS SECTIONS

Cross sections have been measured using the hydrogen data for all final states exhibiting two or more visible decays of strange particles. We use the relationship

$$\sigma=\frac{N_{\text{corr}}}{F},$$

where N_{corr} is the observed number of events corrected for geometric cuts, scanning efficiency,

processing efficiency, probability cutoff (0.1%), loss of events near the beam entrance window, kinematic ambiguity, and visibility factors for neutral decays. (We have used $\frac{2}{3}$ for the fraction of Λ decaying into $p\pi^-$ and $\frac{1}{3}$ for the fraction of observable $K^0 \to \pi^-\pi^+$ decays.) The flux factor or effective path length F is

$$F = N_0 \lambda (1 - e^{-L/\lambda}) N_A \rho = 30 \pm 1 \text{ events}/\mu\text{b}.$$

Here, N_0 is the number of K^- beam tracks measured by sample counting and corrected for π^- and μ^- contamination, N_A is Avogadro's number, ρ is the hydrogen density measured using $\pi \to \mu \to e$ decays, and L is the average path length of a beam track in the fiducial region. The K^- mean free path in the bubble chamber λ has been computed from the relationship

$$\lambda = \frac{\lambda_I \lambda_d}{\lambda_I + \lambda_d} ,$$

$$\lambda_I = \frac{A}{N_A \rho \sigma_T} , \quad \lambda_d = P_K (c\tau_K)/M_K ,$$

where A is the atomic number of the target fluid, $\sigma_T = 26.65 \pm 0.90$ mb is the total $K^- p$ cross section at our beam momentum, and P_K, M_K, and τ_K are the momentum, mass, and lifetime, respectively, of the K^- beam.

The geometric weighting procedure, which accounts for the finite size of our fiducial volume and the losses of events due to short projected length or small projected opening angle of charged and neutral decays, has been described elsewhere.[13] The average geometric weight for events of this experiment is 1.70. Our scanning efficiency, averaged over all topologies, has been estimated on the bases of third scans and analysis with the visibility-dependent Derenzo-Hildebrand technique[14] to be $(84 \pm 7)\%$. Although this is considerably lower than the efficiency calculated using the standard double-scan procedure (~97%), our studies indicate that it more closely represents the true efficiency for the complex topologies encountered here. From the fractions of events reaching our final sample in each of two successive passes through the measuring and processing procedure, and from a study of those events which failed to reach our final sample after several measurements, we have computed a processing efficiency of $(93 \pm 3)\%$, averaged over all topologies. Altogether, the net channel-averaged correction factor for the events of this experiment, which includes scanning efficiency, processing efficiency, probability cutoff, and loss of events near the beam entrance window, is 1.35 ± 0.12.

Our results for all channels having a fully corrected cross section of 1.0 μb or greater are presented in Table IV. An internal check on our procedures is provided by comparing the same reaction cross section obtained from different topologies ($\Xi^-\pi^+K^0$ from $\Xi_1^-\pi^+K_1^0$, $\Xi_1^-\pi^+K_2^0$, and $\Xi_2^-\pi^+K_1^0$; $\Xi^-\pi^+K^0\pi^0$ from $\Xi_1^-\pi^+K_1^0\pi^0$ and $\Xi_2^-\pi^+K_1^0\pi^0$). Here, as was the case for the K^-n cross sections previously published,[1] the cross sections derived from topologies involving three visible decays of strange particles are reduced relative to those with only two visible decays. A study[1] of this problem has indicated that the loss of events is likely to be due to the combined effects of reduced scanning and processing efficiencies for these highly constrained final states. The $\Xi_1^-\pi^+K_1^0$ and $\Xi_1^-\pi^+K_1^0\pi^0$ cross sections should therefore be considered as lower limits for the topology, and the $\Xi_1^-\pi^+K_2^0$, $\Xi_2^-\pi^+K_1^0$, and $\Xi_2^-\pi^+K_1^0\pi^0$ cross sections should be understood to contain a systematic overestimate, due to misidentified $\Xi_1^-K_1^0(\pi)$ events, not exceeding the statistical errors quoted. The effect on our average scanning and processing efficiencies of the small number of events having three visible decays is negligible.

The cross section for the reaction $K^-p \to \Lambda_1 K_1^0 K_2^0$ requires special consideration since there is the possibility of contamination from the underconstrained reactions $K^-p \to \Xi_1^0 K_1^0 \pi^0$ and $K^-p \to \Sigma_1^0 K_1^0 K_2^0$. Assuming similar production characteristics for the reactions $K^-p \to \Xi^0\pi^0K^0$ and $K^-p \to \Xi^-\pi^+K^0$, and using Monte Carlo generated distributions for $M(K^0\gamma)$ and $M(\pi^0\pi^0)$ in the final states $\Sigma_1^0K_1^0K_2^0$ and $\Xi_1^0K_1^0\pi^0$, an analysis of the measured recoil-mass spectrum $[K^-p \to \Lambda_1 K_1^0(\text{MM})]$ yields the following best estimate of the composition of our 467-event $\Lambda_1K_1^0K_2^0$ sample.

417 ± 22 $\Lambda_1 K_1^0 K_2^0$

30 ± 10 $\Xi_1^0 K_1^0 \pi^0$

20 ± 6 $\Sigma_1^0 K_1^0 K_2^0$

An independent analysis, based upon estimated production cross sections for the final states $\Sigma_1^0K_1^0K_2^0$ and $\Xi_1^0K_1^0\pi^0$, Monte Carlo calculations[15] of the fractions of these events fitting the $\Lambda_1K_1^0K_2^0$ hypothesis, and geometric factors for the $\Lambda_1K_1^0$ topology, yields contamination levels consistent with those above. Consequently a subtraction of 50 events has been made in obtaining the $\Lambda_1K_1^0K_2^0$ cross section quoted in Table IV.

Also contained in Table IV are the cross sections for the final states ΛK^-K^+ and $\Sigma^0K^-K^+$. The appropriate correction factors for the two-prong-plus-V^0 scan have been discussed elsewhere.[16] Our inability to clearly resolve ambiguities and estimate losses precludes determination of a cross section for the final state $\Xi_1^0\pi^-K^+$.

The procedure used for cross-section calcula-

TABLE IV. Cross sections from hydrogen experiment.

Topology	No. of events [a]	Weighted no. of events [b]	Topological cross section (μb)	Reaction final state	Cross section [c] (μb)
$\Xi_1^0 K_1^0$	32 (3)	49 ± 11	2.2 ± 0.5	$\Xi^0 K^0$	9.9 ± 2.3
$\Xi_1^- K^+$	316 (1)	507 ± 34	23.1 ± 2.7	$\Xi^- K^+$	34.7 ± 4.1
$\Xi_1^- \pi^+ K_1^0$	148 (0)	251 ± 27	11.2 ± 1.6 [f]	$\Xi^- \pi^+ K^0$	50.4 ± 7.2 [f]
$\Xi_1^- \pi^+ K_2^0$	464 (84)	625 ± 38	28.0 ± 3.2	$\Xi^- \pi^+ K^0$	63.0 ± 7.1 [g]
$\Xi_2^- \pi^+ K_1^0$	178 (0)	156 ± 15	7.3 ± 1.0	$\Xi^- \pi^+ K^0$	65.7 ± 9.0 [g]
$\Xi_1^- \pi^0 K^+$	373 (84)	453 ± 30	20.3 ± 2.4	$\Xi^- \pi^0 K^+$	30.4 ± 3.5
$\Xi_1^0 \pi^- \pi^+ K_1^0$	108 (24)	133 ± 16	6.0 ± 0.9	$\Xi^0 \pi^- \pi^+ K^0$	26.9 ± 4.2
$\Xi_1^- \pi^- \pi^+ K^+$	139 (0)	194 ± 19	8.7 ± 1.2	$\Xi^- \pi^- \pi^+ K^+$	13.0 ± 1.8
$\Xi_1^- \pi^+ \pi^0 K_1^0$	64 (0)	84 ± 13	3.8 ± 0.7 [f]	$\Xi^- \pi^+ \pi^0 K^0$	16.9 ± 3.0 [f]
$\Xi_2^- \pi^+ \pi^0 K_1^0$	72 (3)	74 ± 11	3.3 ± 0.6	$\Xi^- \pi^+ \pi^0 K^0$	29.8 ± 5.2 [g]
$\Lambda_1 K_1^0 K_2^0$	467 (0)	480 ± 25 [d]	21.6 ± 2.3 [d]		
$\Lambda_1 K_1^0 K_1^0$	47 (0)	52 ± 9	2.4 ± 0.5		
$\Lambda_2 K_1^0 K_1^0$	40 (14)	26 ± 6	1.2 ± 0.3		
$\Lambda_1 K_1^0 K_1^0 \pi^0$	14 (0)	20 ± 6	0.89 ± 0.27		
$\Lambda_1 K_1^0 K^+ \pi^-$	37 (9)	41 ± 8	1.8 ± 0.4	$\Lambda \bar{K}^0 K^+ \pi^-$	8.2 ± 1.7
$\Lambda_1 K^- K_1^0 \pi^+$	51 (16)	51 ± 8	2.3 ± 0.4	$\Lambda K^0 K^- \pi^+$	10.4 ± 1.9
$\Sigma^- \bar{K}_1^0 K^+$	87 (4)	90 ± 12	4.0 ± 0.7	$\Sigma^- \bar{K}^0 K^+$	12.1 ± 2.0
$\Sigma^+ K^- K_1^0$	55 (5)	72 ± 13	3.2 ± 0.7	$\Sigma^+ K^- K^0$	9.7 ± 2.0
$\Sigma_2^0 K_1^0 K_1^0$	26 (14)	21 ± 6	0.94 ± 0.26		
$\Sigma^- K_1^0 K_2^0 \pi^+$	54 (1)	60 ± 10	2.7 ± 0.5		
$\Sigma^+ K_1^0 K_2^0 \pi^-$	41 (3)	45 ± 10	2.0 ± 0.5		
$\Sigma_1^0 K^- K_1^0 \pi^+$	15 (5)	15 ± 5	0.68 ± 0.22	$\Sigma^0 K^- K^0 \pi^+$	3.1 ± 1.0
$\Sigma_1^0 \bar{K}_1^0 K^+ \pi^-$	9 (6)	8 ± 3	0.34 ± 0.14	$\Sigma^0 \bar{K}^0 K^+ \pi^-$	1.5 ± 0.6
$\Lambda_1 K^- K^+$	723 (0)	779 ± 30	50.6 ± 3.4	$\Lambda K^- K^+$	76 ± 5
$\Sigma_1^0 K^- K^+$	e	e	15.2 ± 1.8 [e]	$\Sigma^0 K^- K^+$	22.9 ± 2.7 [e]

[a] Total number of events (number of unresolved ambiguities).
[b] Corrected for geometric detection efficiency and ambiguities.
[c] Corrected for neutral decays. The errors quoted are purely statistical.
[d] Estimated contamination has been subtracted (see text).
[e] This final state contains an exceptionally large number of resolved ambiguities. The cross sections are based upon a final sample of 197 selected events (see text), and have been corrected for possible loss into the final state $\Lambda K^- K^+ \pi^0$ (see text).
[f] Cross section not reliable (see text).
[g] Contains a systematic overestimate not exceeding the statistical errors quoted (see text).

tions in the deuterium experiment has been reported previously.[1] As a check, we can compare the cross sections for those reaction channels which contain no missing neutrals other than the spectator neutron. The results, contained in Table V, are in good agreement with the hydrogen data.

V. EVIDENCE FOR Ξ^* PRODUCTION

We present here the results of our search for evidence of production of higher-mass Ξ^* resonances in the final-state mass distributions of reactions (2)–(14). We do not expect, and have not found, biases associated with combining the data

TABLE V. Cross sections from deuterium experiment.

Topology	No. of events [a]	Weighted no. of events [b]	Topological cross section (μb)	Reaction final state	Cross section (μb) [c]
$\Xi_1^- K^+$	170 (0)	291 ± 28	26.1 ± 3.3	$\Xi^- K^+$	39.2 ± 5.0
$\Xi_1^- \pi^+ K_1^0$	91 (0)	103 ± 16	9.8 ± 1.9 [d]	$\Xi^- \pi^+ K^0$	44.1 ± 8.6 [d]
$\Xi_2^- \pi^+ K_1^0$	95 (0)	93 ± 12	8.7 ± 1.4	$\Xi^- \pi^+ K^0$	78.3 ± 12.6 [e]
$\Xi_1^- \pi^- \pi^+ K^+$	80 (0)	100 ± 13	9.5 ± 1.6	$\Xi^- \pi^- \pi^+ K^+$	14.3 ± 2.4
$\Lambda_1 K_1^0 K_1^0$	15 (0)	17 ± 5	1.6 ± 0.5		
$\Lambda_1 \bar{K}_1^0 K^+ \pi^-$	21 (4)	23 ± 6	2.2 ± 0.6	$\Lambda \bar{K}^0 K^+ \pi^-$	9.9 ± 2.7
$\Lambda_1 K^- K_1^0 \pi^+$	29 (4)	34 ± 7	3.3 ± 0.7	$\Lambda K^- K^0 \pi^+$	14.9 ± 3.2
$\Sigma^- \bar{K}_1^0 K^+$	45 (0)	67 ± 12	6.3 ± 1.3	$\Sigma^- \bar{K}^0 K^+$	18.9 ± 3.9
$\Sigma^+ K^- K_1^0$	24 (0)	29 ± 8	2.8 ± 0.9	$\Sigma^+ K^- K^0$	8.4 ± 2.7

[a] Total number of events (number of unresolved ambiguities) in a subsample of the exposure amounting to 15.8 ± 0.4 events/μb.

[b] Corrected for geometric detection efficiency and ambiguities.

[c] Corrected for neutral decays. The errors quoted are purely statistical.

[d] Cross section not reliable (see text).

[e] Contains a systematic overestimate not exceeding the statistical errors quoted (see text).

from the hydrogen and the deuterium exposures for final states containing no missing neutrals at the production vertex other than the spectator neutron. Furthermore, in those channels which contain an additional missing neutral and which have been fitted in deuterium by assuming a stationary proton target, we find no evidence for bias in invariant-mass combinations involving only measured tracks. As quantitative measures of the compatibility of the two data samples for such mass combinations, we have formed the following test functions.

i. The χ^2 over the invariant-mass spectrum between the hydrogen and deuterium data

$$\chi^2 = \sum_i \frac{[N_i(H_2) - \alpha N_i(D_2)]^2}{N_i(H_2) + \alpha^2 N_i(D_2)} . \tag{20}$$

The sum in (20) is over all bins in the mass histogram containing five or more events. $N_i(H_2)$, $N_i(D_2)$ are the numbers of events in the ith bin in the hydrogen and deuterium data, respectively, and α (~1.67) is a scale factor reflecting the relative sensitivities of the two experiments.

ii. The invariant-mass-squared stretch function

$$\xi = \frac{M_f^2 - M_m^2}{\sigma(M_m^2)} . \tag{21}$$

M_f, M_m are the effective masses formed from fitted and measured variables, respectively, and $\sigma(M_m^2)$ is the error in the measured mass squared.

Both the χ^2 test function (20) and the distributions of the variable (21) indicate that mass distributions involving measured tracks are compatible and may be combined without the introduction of any significant biases. The values of χ^2 obtained are consistent with the number of bins over which they are formed, and both the hydrogen and the deuterium data yield distributions in ξ which are symmetric about, and have mean values consistent with, zero. [For example, $M(\Lambda_1 K_1^0)$ in the final state $\Lambda_1 K_1^0 K_2^0$ yields mean values of 0.03 ± 0.04 for the hydrogen data, −0.01 ± 0.07 for the deuterium data.] Since we are primarily interested in mass combinations having strangeness −2, we have no reservations about combining data from the two experiments when that mass combination involves only measured tracks.

The mass-squared test function (21) is, of course, unavailable for mass combinations involving a missing neutral. It is in such combinations that we would expect to see the maximum effect, if any, of biases in the deuterium fitting procedure. The decision whether or not to use such distributions in our analysis has therefore been made separately for each channel considered, using the χ^2 test function (20) and the general compatibility of maximum-likelihood fits to all mass projections.

A. $K^- p \to \Xi^- \pi^+ K^0$

The results of an analysis of 80% of the hydrogen data for this reaction have been reported previously.[2] This channel had been found to be dominated by $\Xi(1530)K^0$ and $\Xi^- K^{*+}(890)$ production,

as well as the production of higher-mass Ξ^* states in the mass interval 1.8–2.0 GeV/c^2 interpretable as either $\Xi(1820)$ and $\Xi(1940)$ or as a single broad resonance. The most interesting feature had, however, been the appearance of a three-standard-deviation signal in the region near 1630 MeV/c^2. No such signal was observed in subsequent experiments[5] at 2.18 GeV/c (Borenstein *et al.*) and at 3.1, 3.3, and 3.6 GeV/c (Ross *et al.*). The latter experiment has, however, produced a signal near 1610 MeV/c^2 in the final state $(\Xi^-\pi^+)\pi^-K^+$, in the reaction $K^-p \to \Xi^0(1610)K^{*0}(890)$. A more recent experiment, at K^- momenta around 2.0 GeV/c,[17] has seen a $\Xi(1630)$ signal close to three standard deviations above background. Their signal, however, disappears at higher beam momenta (2.3 to 2.5 GeV/c).

The data for the $\Xi^-\pi^+K^0$ final state come from three separate topologies:

$$K^-p \to \Xi_1^-\pi^+K_1^0 \quad (22a)$$

$$\to \Xi_2^-\pi^+K_1^0 \quad (22b)$$

$$\to \Xi_1^-\pi^+K_2^0. \quad (22c)$$

The number of events in each topology and the resolution in the $\Xi^-\pi^+$ combined mass for several mass intervals are given in Table VI.

In Figs. 6(a) and 7(a) we show the $\Xi^-\pi^+$ and π^+K^0 combined mass distributions[18] for the full hydrogen sample. Maximum-likelihood fits, using various fixed $\Xi(1630)$ widths[19] and involving production of $\Xi(1530)$, $\Xi(1630)$, $\Xi(1820)$, $\Xi(1940)$, and $K^*(890)$ have been performed. The goodness of the fit is insensitive to the $\Xi(1630)$ width, and the statistical significance of the $\Xi(1630)$ remains unaltered at about three standard deviations; with $\Gamma[\Xi(1630)] = 15$ MeV, the $\Xi(1630)$ fraction is 0.033 ± 0.011, increasing to 0.048 ± 0.016 with $\Gamma[\Xi(1630)] = 30$ MeV. The results for $\Gamma[\Xi(1630)] = 22.5$ MeV are given in Table VII and the corresponding curves are shown in Figs. 6(a) and 7(a).

In Figs. 6(b) and 7(b) we show the corresponding mass distributions obtained from the deuterium experiment. The solid curves, drawn for comparison purposes only, represent the hydrogen fit normalized to the deuterium data. It is clear that high-mass structure, evident in the hydrogen data, is not required here. Indeed, an adequate fit to the $\Xi^-\pi^+$ mass projection ($\chi^2 = 26$ for 29 constraints) can be obtained for this final state assuming only production of $\Xi^0(1530)K^0$ [$(18 \pm 2)\%$] and $\Xi^-K^{*+}(890)$ [$(35 \pm 5)\%$]. The resulting resonance parameters are $M[\Xi^0(1530)] = 1533 \pm 2$ MeV/c^2, $\Gamma[\Xi^0(1530)] = 14 \pm 3$ MeV, $M[K^{*+}(890)] = 889 \pm 6$ MeV/c^2, and $\Gamma[K^{*+}(890)] = 80 \pm 16$ MeV. We note, however, the two-bin excess of events in the mass interval $1.625 < M(\Xi^-\pi^+) < 1.675$ GeV/c^2. In order to estimate its significance in a manner which avoids bias due to known higher-mass Ξ^* effects, we have used phase space normalized to the region $1.575 < M(\Xi^-\pi^+) < 1.775$ GeV/c^2 [dashed curve in Fig. 6(b)]. We obtain a 2.0-standard-deviation signal of 14 events above a background of 33 events. Although this effect obviously cannot be considered sufficient evidence for $\Xi(1630)$, we point out that it represents a second independent sign of activity in the region of 1630 MeV/c^2. In view of the conflicting experimental evidence, the interpretation of this effect remains unclear.

Figures 6(c) and 7(c) represent the combined hydrogen and deuterium $\Xi^-\pi^+$ and π^+K^0 invariant-mass distributions. As is clear from the dashed curve on Fig. 6(c), which represents the distribution expected in the absence of high-mass Ξ^*'s, there is an excess of events having $M(\Xi^-\pi^+) > 1.8$ GeV/c^2. However, fits to the data cannot dis-

TABLE VI. Total numbers of events and $\Xi^-\pi^+$ mass resolution for the reaction $K^-p \to \Xi^-\pi^+K^0$.

Topology	No. of events	$\Xi^-\pi^+$ mass resolution[a] (MeV/c^2) $M(\Xi\pi) < 1.58$	$1.58 < M(\Xi\pi) < 1.80$	$M(\Xi\pi) > 1.80$ GeV/c^2
H_2: $\Xi_1^-\pi^+K_1^0$	148	6	8	15
$\Xi_2^-\pi^+K_1^0$	178	6	12	16
$\Xi_1^-\pi^+K_2^0$	464	6	13	20
Total	790	6	12	18
D_2: $\Xi_1^-\pi^+K_1^0$	96	8	14	20
$\Xi_2^-\pi^+K_1^0$	99	8	16	28
$\Xi_1^-\pi^+K_2^0$	306	8	16	24
Total	501	8	16	24

[a] Full width at half maximum of Gaussian resolution function.

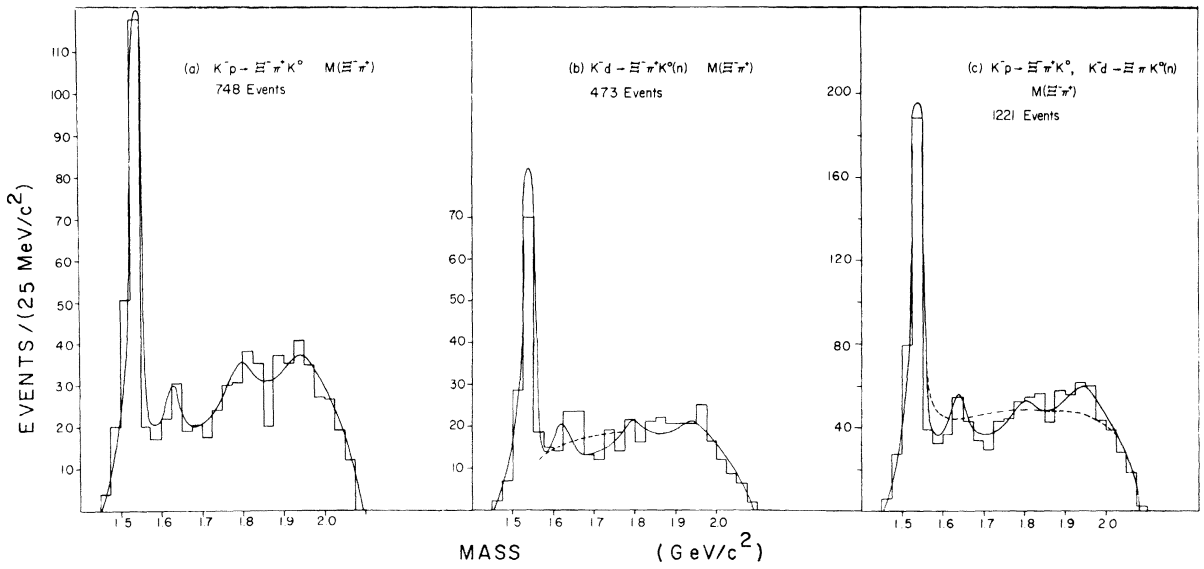

FIG. 6. The $\Xi^-\pi^+$ effective-mass distributions for the reaction $K^-p \to \Xi^-\pi^+K^0$. (a) Hydrogen data. (b) Deuterium data. (c) Combined hydrogen and deuterium data. The solid curves represent fits to the final states $\Xi(1530)K$, $\Xi(1630)K$, $\Xi(1820)K$, $\Xi(1940)K$, $\Xi K^*(890)$, and $\Xi^-\pi^+K^0$. The dashed curve in (b) shows phase space normalized to the region $1.575 < M(\Xi^-\pi^+) < 1.775$ GeV/c^2 (see text). The dashed curve in (c) represents the distribution expected in the absence of high-mass Ξ^* effects.

tinguish between a one- or two-resonance interpretation. We have therefore fixed the masses and widths of $\Xi(1820)$ and $\Xi(1940)$ at the values determined from the hydrogen data alone. The resulting parameters for $\Xi^-(1530)$, $\Xi(1630)$, and $K^*(890)$ are listed in Table VII, and the corresponding solution is displayed in Figs. 6(c) and 7(c).

B. $K^-p \to \Xi^-\pi^0K^+$

Our data samples for this reaction consist of 373 hydrogen events [84 ambiguous with reaction (22c)] and 198 deuterium events [56 ambiguous with reaction (22c)]. Analysis results based upon 80% of the hydrogen data have been published.[2] No evidence for higher-mass Ξ^* resonances was observed, and the data was adequately fitted by the two processes $K^-p \to \Xi^-K^{*+}(890)$ and $K^-p \to \Xi^-(1530)K^+$. The full hydrogen sample yields similar results, with $(27 \pm 6)\%\ \Xi^-K^{*+}(890)$, $M = 898 \pm 7$ MeV/c^2, $\Gamma = 66 \pm 23$ MeV and $(18 \pm 4)\%\ \Xi^-(1530)K^+$, $M = 1541 \pm 6$ MeV/c^2, $\Gamma = 43 \pm 13$ MeV. The experimental $\Xi(1530)$ width reflects the poor $\Xi\pi$ mass resolution in this channel; for a determination of the true $\Xi(1530)$ width see Ref. 19. Figure 8 contains the three mass projections for the

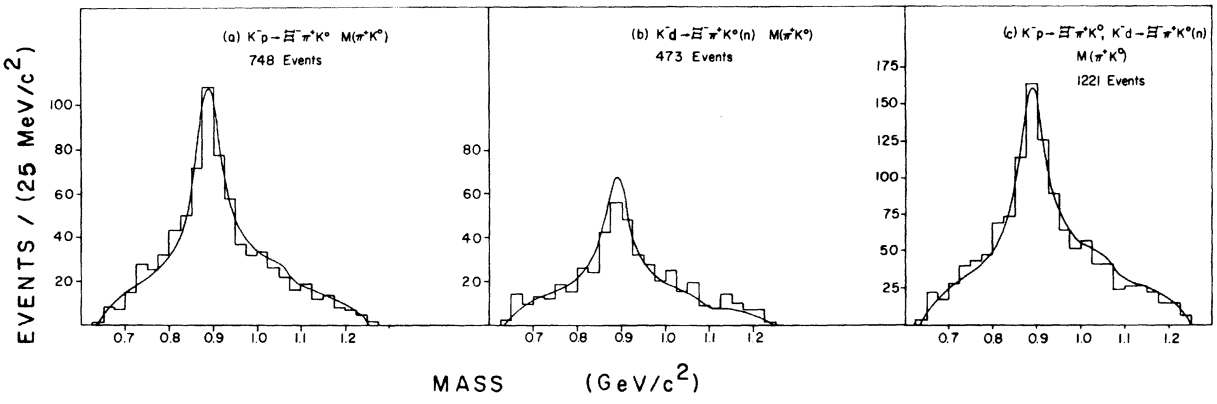

FIG. 7. The π^+K^0 effective-mass distributions for the reaction $K^-p \to \Xi^-\pi^+K^0$. (a) Hydrogen data. (b) Deuterium data. (c) Combined hydrogen and deuterium data. The solid curves represent fits to the final states $\Xi(1530)K$, $\Xi(1630)K$, $\Xi(1820)K$, $\Xi(1940)K$, $\Xi K^*(890)$, and $\Xi^-\pi^+K^0$.

TABLE VII. Fit parameters[a] for the final state $\Xi^-\pi^+K^0$.

Process	Sample	Mass (MeV/c^2)	Width (MeV)	Percent
$\Xi(1530)K$	H_2	1531	13.9 ± 1.9	22 ± 2
	D_2	1533 ± 2	14 ± 3	18 ± 2
	H_2+D_2	1531	15 ± 2	22 ± 2
$\Xi(1630)K$	H_2	1624 ± 2.5	22.5	4.1 ± 1.4
	D_2	...	...	...
	H_2+D_2	1637 ± 7	49 ± 17	6.2 ± 2.4
$\Xi(1820)K$	H_2	1797 ± 19	99 ± 57	9.9 ± 5.9
	D_2	...	...	...
	H_2+D_2	1797	99	7.5 ± 3.1
$\Xi(1940)K$	H_2	1961 ± 18	159 ± 57	18.6 ± 5.6
	D_2	...	...	...
	H_2+D_2	1961	159	17.9 ± 3.8
$\Xi K^*(890)$	H_2	889	71 ± 13	45 ± 5
	D_2	889 ± 6	80 ± 16	35 ± 5
	H_2+D_2	889	74 ± 10	41 ± 4

[a] Underlined quantities were not varied in the fit.

hydrogen data, with the above solution superimposed.

The deuterium data similarly shows no evidence for Ξ* production other than Ξ(1530). The poorer mass resolution due to the deuterium fitting procedure does not make it worthwhile to combine the hydrogen and deuterium samples.

C. $K^-p \to \Xi\pi\pi K$

These final states are contributed by the following four topologies involving a total of 375 hydrogen events and 165 deuterium events:

$$K^-p \to \Xi_1^-\pi^-\pi^+K^+ \quad (23a)$$

$$\to \Xi_1^-\pi^+\pi^0K_1^0 \quad (23b)$$

$$\to \Xi_2^-\pi^+\pi^0K_1^0 \quad (23c)$$

$$\to \Xi_1^0\pi^-\pi^+K_1^0. \quad (23d)$$

The results of an analysis of the complete hydrogen sample has been published.[2] The only prominent feature in the two-body Ξπ systems is Ξ(1530), comprising $(63.8 \pm 5.1)\%$ of the sample. The Ξπ mass distribution above 1575 MeV/c^2 is smooth and shows no sign of other resonant activity. The principal results were 5.0- and 4.3-standard-deviation signals in the Ξ(1530)π effective-mass distributions having masses and widths of 1829 ± 9 MeV/c^2, 52 ± 43 MeV and 1964 ± 10 MeV/c^2, 60 ± 39 MeV, respectively. The solution corresponding to these parameters is displayed over the hydrogen data in Fig. 9. The effect of combining

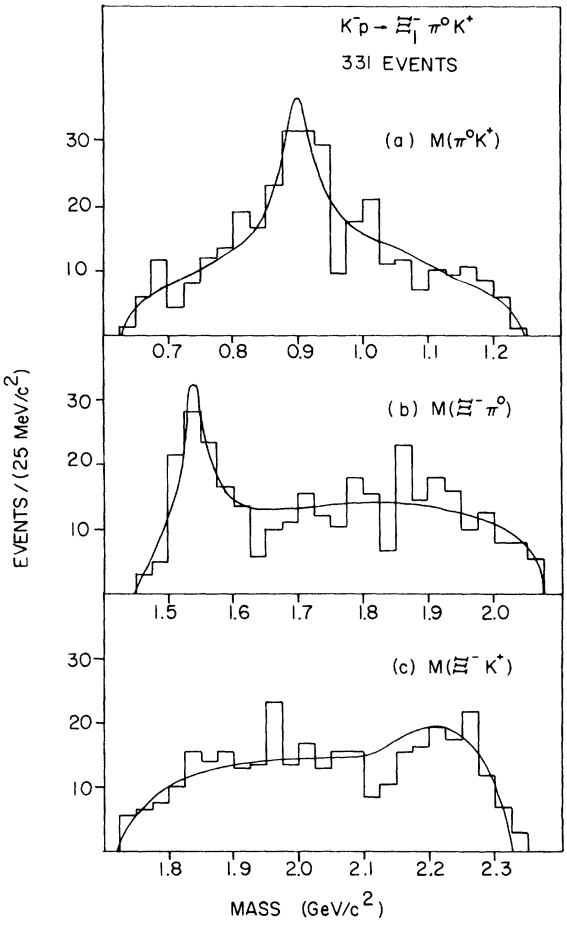

FIG. 8. Effective-mass distributions for the final state $\Xi_1^-\pi^0K^+$ obtained from the hydrogen data alone. (a) $M(K^+\pi^0)$. (b) $M(\Xi^-\pi^0)$. (c) $M(\Xi^-K^+)$. The solid curves represent the best fit to the data using the processes $K^-p \to \Xi^-K^{*+}(890)$, $K^-p \to \Xi^-(1530)K^+$, and $K^-p \to \Xi^-\pi^0K^+$.

the hydrogen data with the final states [(23b)–(23d)] obtained from deuterium is to reduce the resolution of the observed signals. Each of these final states was fitted in deuterium by assuming a stationary proton target, and the missing neutral is involved in the relevant mass combination. Also, no significant change is made to the parameters determined from the hydrogen data when the 87 deuterium events fitting reaction (23a) are added to the sample.

D. $K^-p \to \Xi^0\pi^-K^+$

Our sample of 295 events for this reaction has been obtained from the scan for the two-prong-plus-V^0 topology by requiring a unique fit and applying the selection criteria described in Sec. III. With these criteria we expect a contamination of no more than 16% by the final states $\Sigma^0K^-K^+$ and $\Lambda\pi^-\pi^+X^0$, where $X^0 = \gamma$, π^0, or η. We note,

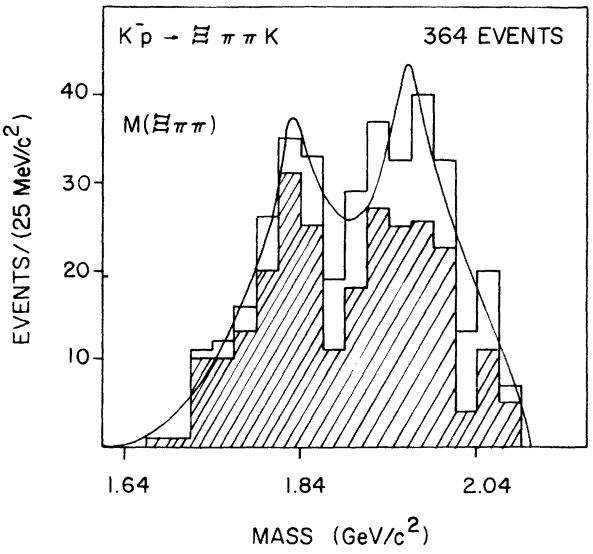

FIG. 9. The $\Xi\pi\pi$ invariant-mass distribution for the final states $\Xi_1^-\pi^+\pi^-K^+$, $\Xi_1^-\pi^+\pi^0K_1^0$, $\Xi_2^-\pi^+\pi^0K_1^0$, and $\Xi_1^0\pi^-\pi^+K_1^0$. The shaded area represents the events involving production of $\Xi(1530)$. For a full discussion of the analysis of these channels, see Ref. 2.

however, the possibility that a substantial number of events have been rejected from our sample due to an ambiguity with the latter set of reactions. After examination of the ambiguous events, we find ourselves unable to discriminate between $\Xi^0\pi^-K^+$ and the competing hypotheses. However, examination of the invariant-mass spectra for the rejected events, and Monte Carlo studies of the consequences of such a selection, indicate that although the low- and high-mass regions of the $\Xi^0\pi^-$ and Ξ^0K^+ mass distributions may be depleted relative to the central regions, any biases introduced will not significantly affect the results described below. In particular, no peaks are generated by these selections.

Figures 10(a)–10(c) contain the three invariant-mass projections for this final state. The obvious features are production of $K^*(890)$, $\Xi(1530)$, and, as can be see from the Dalitz plot of Fig. 10(d), correlated high-mass $\Xi^0\pi^-$ and low-mass Ξ^0K^+ peaks. Similar peaking in $M(\Xi K)$ near 1960 MeV/c^2, correlated with a high-mass ($\simeq$1900 MeV/c^2) excess in $M(\Xi\pi)$, had been observed in the reactions $K^-n \to \Xi^{-(0)}\pi^{0(-)}K^0$ obtained from the deuterium exposure of these experiments.[1] Although fits to that data were improved by inclusion of a $\Sigma(1960)$ ($M = 1963 \pm 10$ MeV/c^2, $\Gamma = 67 \pm 43$ MeV), the absence of such a signal in the reaction $K^-n \to \Xi^-\pi^-K^+$ led us to explain this effect in terms of known high-mass Ξ resonances.

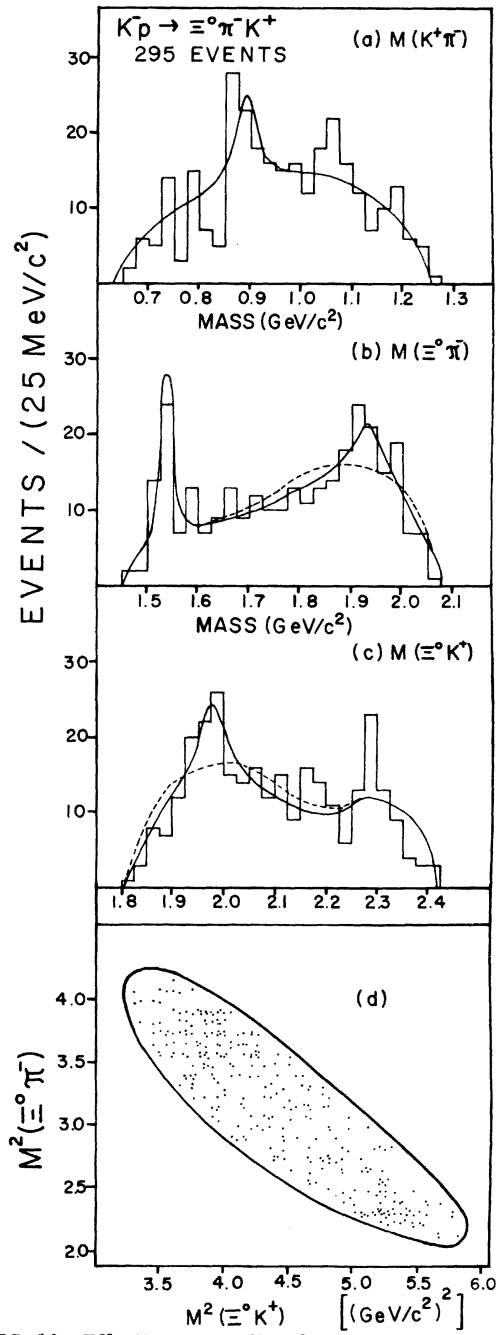

FIG. 10. Effective-mass distributions and Dalitz plot for the final state $\Xi^0\pi^-K^+$. (a) $M(K^+\pi^-)$. (b) $M(\Xi^0\pi^-)$. (c) $M(\Xi^0K^+)$. (d) Dalitz plot for the two baryonic mass combinations. The dashed curves are explained in the text. The solid curve represents our final fit to the data, which involves the final states $\Xi^0K^{*0}(890)$, $\Xi^-(1530)K^+$, $\Xi^-(1940)K^+$, $\Sigma^+(1960)\pi^-$, and $\Xi^0\pi^-K^+$.

No such low-mass peak is observed in $M(\Xi^-K^0)$ from $K^-p \to \Xi^-\pi^+K^0$ reactions (not shown), and the Ξ^-K^+ spectrum from $K^-p \to \Xi^-\pi^0K^+$ reactions shows only a single-bin fluctuation at $M(\Xi^-K^+)$

$= 1960$ MeV/c^2 [Fig. 8(c)]. However, in these channels K^* exchange, which is the most likely mechanism for Σ^* production, is exotic or isotopic-spin suppressed; consequently we would not expect to observe Σ^* production. Peripheral behavior as expected from K^* exchange is observed here for the events having $1.900 < M(\Xi^0 K^+) < 2.025$ GeV/c^2; however, a control region having $2.075 < M(\Xi^0 K^+) < 2.250$ GeV/c^2 displays similar peripheral peaking. Although no definite conclusions can be drawn, we have included the Σ^* in some of the fits of this final state.

We have performed maximum-likelihood fits to the data in which we have included the final states $\Xi^0 K^{*0}(890)$ and $\Xi^-(1530)K^+$ (with the masses of both resonant systems fixed at their nominal values), as well as production of a high-mass Ξ^* and a low-mass Σ^*. The dashed curve on Fig. 10(c) shows the distribution expected in $M(\Xi^0 K^+)$ if production only of $K^*(890)$, $\Xi(1530)$, and $\Xi(1940)$ are assumed. The resulting $\Xi^-(1940)$ parameters are $(25 \pm 7)\%$, $M = 1938 \pm 15$ MeV/c^2, and $\Gamma = 107 \pm 31$ MeV; and the fitted distributions in $M(K^+\pi^-)$ and $M(\Xi^0\pi^-)$ do not differ greatly from the solid curves shown on Figs. 10(a), 10(b). What is to be noted is that there remains a 2.9-standard-deviation excess of events in the mass interval $1.925 < M(\Xi^0 K^+) < 2.00$ GeV/c^2. Alternatively, if we treat the correlated peaks as pure Σ^* production, we obtain the $\Xi^0\pi^-$ distribution indicated by the dashed curve in Fig. 10(b), which is 2.3 standard deviations below the observed spectrum in the interval $1.875 < M(\Xi^0\pi^-) < 1.950$ GeV/c^2. The resulting Σ^* parameters are $(26 \pm 10)\%$, $M = 1981 \pm 31$ MeV/c^2, and $\Gamma = 104 \pm 59$ MeV. Again, the distributions in $M(K^+\pi^-)$ and $M(\Xi^0 K^+)$ for this solution follow closely the solid curves in Figs. 10(a), 10(c).

Clearly the best fit, to which the solid curves in Fig. 10 correspond, is obtained when both $\Xi(1940)$ and Σ^* production are assumed. The resonance parameters corresponding to this solution are

$M[\Xi(1940)] = 1936 \pm 22$ MeV/c^2,

$\Gamma[\Xi(1940)] = 87 \pm 26$ MeV,

$\%[\Xi(1940)] = 14.8 \pm 6.3$;

$M(\Sigma^*) = 1979 \pm 14$ MeV/c^2,

$\Gamma(\Sigma^*) = 69 \pm 32$ MeV,

$\%(\Sigma^*) = 14.3 \pm 6.6$;

$\%[K^*(890)] = 11.3 \pm 4.1$,

$\Gamma[K^*(890)] = 43 \pm 14$ MeV;

$\%[\Xi(1530)] = 10.1 \pm 3.1$,

$\Gamma[\Xi(1530)] = 20 \pm 10$ MeV.

The best explanation of the data, then, seems to require production of $\Xi^-(1940) \to \Xi^0\pi^-$ and $\Sigma^*(1960) \to \Xi^0 K^+$, even though neither signal achieves the three-standard-deviation significance level. The Particle Data Group[20] lists a Σ^* having a mass not inconsistent with that observed here (1900 to 1960 MeV/c^2), and having a substantial unobserved branching fraction. High-mass Ξ signals have of course been observed before, primarily in the final state $\Xi^-\pi^+K^0$, and more recently by the Oxford group[21] in the combined final states $\Xi^{-(0)}\pi^{0(-)}K^+$. Their signal, coming mainly from the $\Xi^0\pi^-K^+$ final state, had a mass of 1952 ± 11 MeV/c^2 and a width of 38 ± 10 MeV. However, lack of discussion of ambiguities, or of the corresponding $\Xi^0 K^+$ mass spectrum, makes a direct comparison difficult.

E. $K^-p \to \Lambda \bar{K}^0 K^0$

The primary sources of events for this reaction are the topologies $\Lambda_1 K_1^0 K_2^0$ (467 events in hydrogen, 281 events in deuterium) and $\Lambda_1 K_1^0 K_1^0$ (47 and 15 events in hydrogen and deuterium, respectively). Owing to the large ambiguity rate with the final state $\Sigma_2^0 K_1^0 K_1^0$, the topology $\Lambda_2 K_1^0 K_1^0$ has not been included in our analysis.

As is evident in the $K_1^0 K_2^0$ mass projections of Fig. 11, the final state $\Lambda_1 K_1^0 K_2^0$ is dominated by

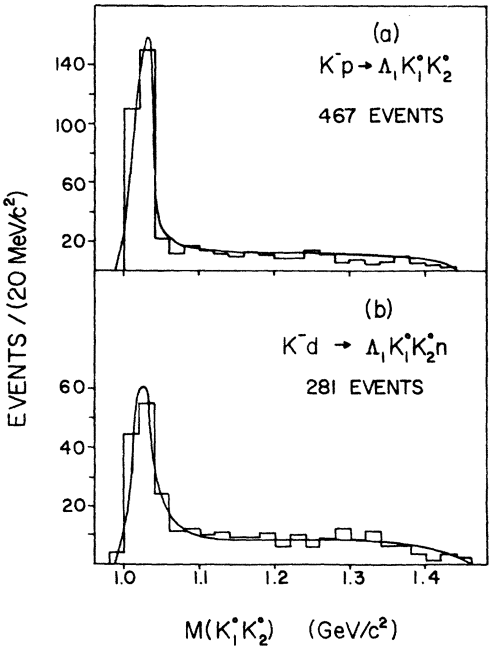

FIG. 11. The $K_1^0 K_2^0$ invariant-mass distributions for the final state $\Lambda K_1^0 K_2^0$. (a) Hydrogen data. (b) Deuterium data. The solid curves represent fits to this final state using $\Lambda\phi(1019)$ production plus phase space.

the quasi-two-body process $K^-p \to \Lambda\phi(1019)$. We have found that adequate separation between production of $\phi(1019)$ and other processes is attained by restricting $M(K_1^0K_2^0) > 1.05$ GeV/c^2. From the number of ϕ resonant events in hydrogen and deuterium we obtain the following topological cross sections: 13.8 ± 1.6 μb in hydrogen and 14.2 ± 2.3 μb in deuterium for the reaction $K^-p \to \Lambda\phi \to \Lambda_1 K_1^0 K_2^0$. We note, however, that the percentage of ϕ resonant events is substantially smaller in deuterium [$(49.9 \pm 1.4)\%$ versus $(63.9 \pm 2.7)\%$ in hydrogen], indicating the presence of a substantial contamination of background events in the deuterium sample due to the fitting procedure used. Because of this large contamination we shall restrict our Ξ^* analysis to the measured combination $\Lambda_1 K_1^0$ in the deuterium sample.

Attempts to extract the process $K^-p \to \Xi^{*0}K^0$, $\Xi^{*0} \to \Lambda\bar{K}^0$ from these final states are complicated by the following two factors:

(i) The possibility of contamination by the underconstrained reactions $K^-p \to \Xi_1^0\pi^0K_1^0$ and $K^-p \to \Sigma_1^0K_1^0K_2^0$ fitted as $K^-p \to \Lambda_1K_1^0K_2^0$.

(ii) The inability to distinguish $\bar{K}^0$ decay from K^0 decay, which renders the strangeness-(−2) mass combination ambiguous and admits the possibility of N^* signals from the process $K^-p \to N^*\bar{K}^0$, $N^* \to \Lambda K$ in our ΛK^0 spectrum.

The contamination mentioned in (i) has been checked with Monte Carlo generated events. We have found that those reactions will produce a smooth background in the ΛK^0 combined mass distribution which is consistent with ΛK^0 phase space. A more serious problem is the possibility of a shifted peak in ΛK^0 due to the reaction $K^-p \to \Xi^{*0}K^0$, $\Xi^{*0} \to \Sigma^0\bar{K}^0$. We can, however, use the final state $\Sigma^+K^-K_1^0$ to measure the production cross section of such a Ξ^*. The upper limit of 1.1 μb found there corresponds to less than 12 $K^-p \to \Xi^{*0}K^0$, $\Xi^{*0} \to \Sigma_1^0\bar{K}^0$ events in the combined hydrogen and deuterium experiments.

In order to resolve the difficulties mentioned in (ii), we have made use of conventional expectations for meson exchange in N^* production and for baryon exchange in production of Ξ^*. By requiring that the (ΛK^0) system be forward in the overall center-of-mass system, $N^*\bar{K}^0$ production should be minimized and Ξ^* production enhanced relative to background.[22]

We therefore show in Fig. 12 the distribution in $M(\Lambda K^0)_{\text{forward}}$ for the combined data sample after removal of events involving production of $\phi(1019)$ [$M(K_1^0K_2^0) < 1.05$ GeV/c^2]. Deuterium events in which the forward ΛK^0 combination involves a K_2^0 have been excluded. The hydrogen data are shown shaded. The enhancement in the interval $1.84 \leq M(\Lambda K^0) \leq 1.92$ GeV/c^2 is three standard deviations above background, and a maximum-likelihood fit of this mass projection to Ξ^*K^0 production plus phase space yields $(20 \pm 6)\%$ production of a Ξ^* with a mass of 1870 ± 9 MeV/c^2 and a width of 44 ± 11 MeV. No evidence exists for this signal in $M(\Lambda K^0)_{\text{backward}}$ in either the hydrogen or the deuterium samples. A similar fit to the hydrogen data alone yields $M = 1865 \pm 9$ MeV/c^2 and $\Gamma = 31 \pm 10$ MeV, with the signal comprising $(18 \pm 6)\%$ of the 158 events.

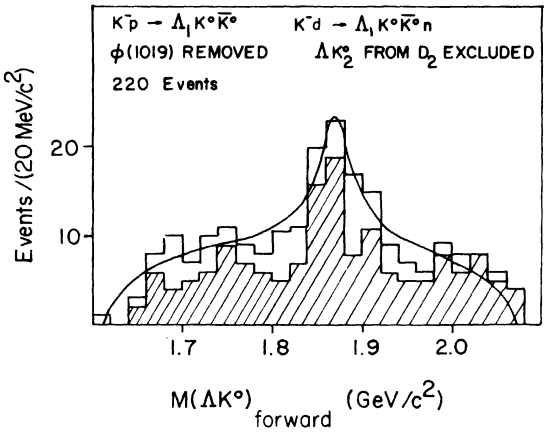

FIG. 12. Effective-mass distribution of forward ΛK^0 combinations in the final state $\Lambda\bar{K}^0K^0$, for the combined hydrogen and deuterium sample. If both ΛK^0 combinations are forward in the overall center-of-mass frame, the more forward one is chosen. Deuterium events in which this combination involves a K_2^0, and all events involving production of $\phi(1019)$, are excluded. The shaded portion represents hydrogen data alone. The curve represents the best fit to production of $\Xi^{*0}K^0$.

F. $K^-p \to \Lambda K^-K^+$

As with the final state $\Lambda\bar{K}^0K^0$, the dominant feature of the 723 events fitting this reaction is quasi-two-body production of $\phi(1019)$ [Fig. 13(a)]. Here, however, the strangeness-(−2) combination is unique, and we show in Fig. 13(b) the invariant-mass distribution $M(\Lambda K^-)$ both before and after (shaded portion) removal of events having $M(K^-K^+) < 1.05$ GeV/c^2. Both distributions exhibit an enhancement consistent with $\Xi(1820)$ signals observed in this mass region in previous experiments[3] and in the reaction $K^-n \to \Lambda K^-K_1^0$ obtained from the deuterium exposure of this experiment.[1] A maximum-likelihood fit of this final state to the processes $K^-p \to \Lambda\phi(1019)$, $K^-p \to \Xi^-(1820)K^+$, and $K^-p \to \Lambda K^-K^+$ yields the following resonance parameters:

$$M[\phi(1019)] = 1019.4 \pm 0.4 \text{ MeV}/c^2,$$

$$\Gamma[\phi(1019)] = 7.5 \pm 0.6 \text{ MeV},$$

$\%[\Lambda\phi(1019)] = 55 \pm 2.2$;

$M[\Xi^-(1820)] = 1813 \pm 4$ MeV/c^2,

$\Gamma[\Xi^-(1820)] = 26 \pm 11$ MeV,

$\%[\Xi^-(1820)K^+] = 7.9 \pm 2.3$.

Also evident in Fig. 13(b) is a peak at 1890 MeV/c^2 which remains a 2.5-standard-deviation effect after removal of $\phi(1019)$. However, when we make the further selection $\hat{K}^+ \cdot \hat{K}^-_{\text{beam}} < 0.0$, shown fully shaded in Fig. 13(b), this apparent signal disappears, whereas the $\Xi(1820)$ signal stands approximately four standard deviations above background.

It is clear that we are observing production and decay of $\Xi^-(1820)$. Using the resonance production fractions determined by the fit, we obtain cross sections of 4.0 ± 1.2 μb and 28.1 ± 2.3 μb, respectively, for the reactions $K^-p \to \Xi^-(1820)K^+$, $\Xi^-(1820) \to \Lambda_1 K^-$ and $K^-p \to \Lambda_1\phi(1019)$, $\phi(1019)$

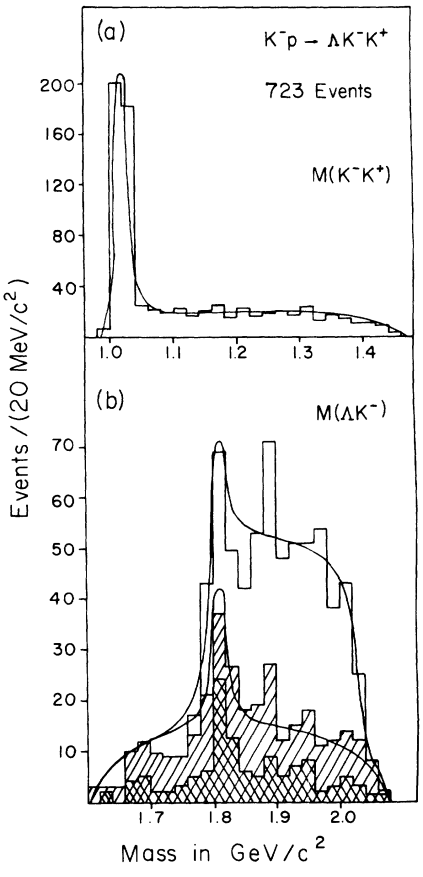

FIG. 13. Distributions in (a) $M(K^-K^+)$ and (b) $M(\Lambda K^-)$ for the final state ΛK^-K^+. The shaded portion of (b) represents the events remaining after removal of $\phi(1019)$. The fully shaded portion of (b) results from the further restriction to forward (ΛK^-) systems. The curves represent the best fit using the processes $K^-p \to \Lambda\phi(1019)$, $K^-p \to \Xi^-(1820)K^+$, and $K^-p \to \Lambda K^-K^+$.

$\to K^-K^+$. The latter cross section is in excellent agreement with that obtained in the $\Lambda_1 K_1^0 K_2^0$ channel; after correction for the alternate decay modes of the $\phi(1019)$ and unseen decays of the Λ we obtain 89 ± 11 μb and 90 ± 9 μb for the reaction $K^-p \to \Lambda\phi$, in the final states $\Lambda_1 K_1^0 K_2^0$ and $\Lambda_1 K^-K^+$, respectively.

G. $K^-p \to \Sigma^-\bar{K}^0K^+$

Figure 14(a) contains the $\Sigma^-\bar{K}^0$ mass projection for the 85 hydrogen events in this final state. 55% of the events are clustered in the mass interval $1.80 < M(\Sigma^-\bar{K}^0) < 1.90$ GeV/c^2, and the Chew-Low plot of Fig. 15 indicates that they are produced preferentially with low-momentum transfer. The shaded portion of Fig. 14(a) corresponds to events having $\hat{K}^+ \cdot \hat{K}^-_{\text{beam}} < 0$. The results of maximum-likelihood fits of both the full sample of events, and the restricted sample having $\hat{K}^+ \cdot \hat{K}^-_{\text{beam}} < 0.0$, to $\Xi^{*-}K^+$ production plus phase space are shown in Table VIII. The curve in Fig. 14(a) represents the fit to the shaded events. For either sample the signal represents a better than three-standard-deviation effect having nominal mass and width of 1860 MeV/c^2 and 60 MeV, respectively.

The deuterium data, however, shown in Fig. 14(b), yields 50 events in which there is no evidence for production of $\Xi(1860)$ in the $\Sigma^-\bar{K}^0$ invariant-mass distribution. We obtain an upper limit of 0.81 μb at the 90% confidence level for production of $\Xi(1860)$ in the mass interval $1.80 < M(\Sigma^-\bar{K}^0) < 1.90$ GeV/c^2. This is not inconsistent with the hydrogen data, being 1.4 standard deviations below the production cross section observed there (see Table VIII). Moreover, the events in the region of 1860 MeV/c^2 exhibit, as with the hydrogen events, a preference for forward production of the $\Sigma^-\bar{K}^0$ system. For these reasons we show in Fig. 14(c) the distribution in $M(\Sigma^-\bar{K}^0)$ for the combined data sample. As expected, the statistical significance of the signal is reduced in the combined data. A maximum-likelihood fit yields $(27 \pm 12)\%$ $\Xi^{*-}K^+$ (see Table VIII), or 2.3 standard deviations. However, as is evident in Fig. 16, which contains the differential cross section for the events having $1.80 < M(\Sigma^-\bar{K}^0) < 1.90$ GeV/c^2, and in the shaded portion of Fig. 14(c) $(\hat{K}^+ \cdot \hat{K}^-_{\text{beam}} < 0)$, a signal with strong preference for forward production exists in the data. The solid curve in Fig. 14(c) represents a fit to the events having $\hat{K}^+ \cdot \hat{K}^-_{\text{beam}} < 0$. It indicates production of a Ξ^* having mass 1860 ± 14 MeV/c^2, width 72 ± 17 MeV, and a topological production cross section of 1.42 ± 0.47 μb.

The mass and width observed here are consistent, within one standard deviation, with the signal

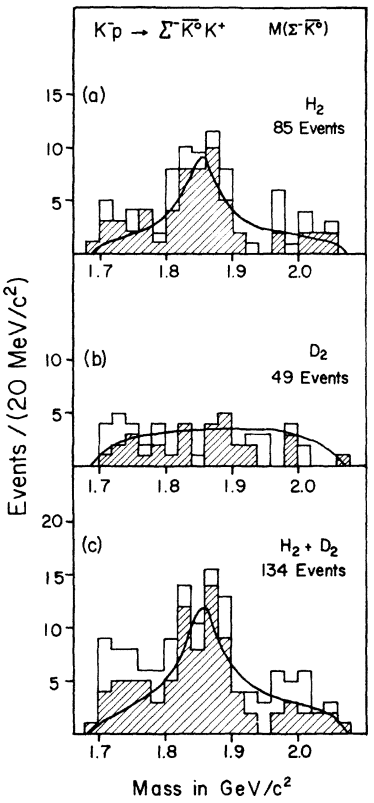

FIG. 14. The $\Sigma^-\bar{K}^0$ effective-mass distributions for the final state $\Sigma^-\bar{K}^0K^+$. (a) Hydrogen data. (b) Deuterium data. (c) Combined hydrogen and deuterium data. The shaded portions correspond to the selection $\hat{K}^+ \cdot \hat{K}^-_{\text{beam}} < 0.0$. The curves in (a) and (c) are fits of Ξ^* production to the shaded events. The curve in (b) is phase space normalized to the complete sample.

observed in the final state $\Lambda\bar{K}^0K^0$. If these signals represent production of the same Ξ resonant state, we obtain 1867 ± 8 MeV/c^2 and 52 ± 9 MeV for the weighted average mass and width, respectively.

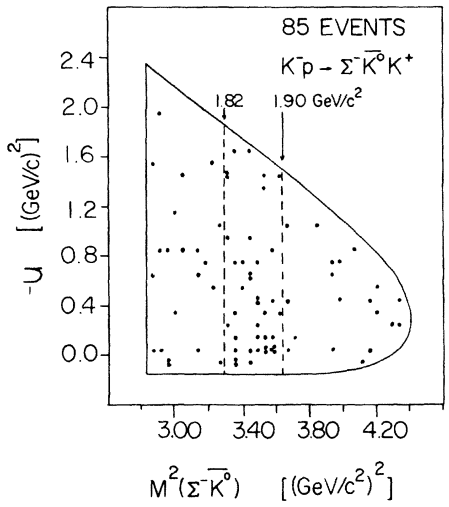

FIG. 15. The Chew-Low plot for the final state $\Sigma^-\bar{K}^0K^+$ in hydrogen.

H. $K^-p \to \Sigma^0K^-K^+$

The K^-K^+ and Σ^0K^- effective-mass distributions for the 197 events accepted into this final state are shown in Fig. 17. The data, obtained from the hydrogen exposure alone, were extracted from a highly ambiguous sample of two-prong-plus-V^0 events and contains only 28% with a unique fit to this reaction. The distributions are adequately fitted assuming only production of $\phi(1019)$ in the reaction $K^-p \to \Sigma^0\phi(1019)$, and phase space. The $\phi(1019)$ fit parameters are $(45 \pm 4)\%$ $K^-p \to \Sigma^0\phi$, with $M = 1019.9 \pm 0.3$ MeV/c^2 and $\Gamma = 4.7 \pm 1.0$ MeV. This solution is superimposed on the mass projections of Fig. 17.

After removal of events involving $\phi(1019)$ [$M(K^-K^+) < 1.05$ GeV/c^2], we obtain the Σ^0K^- mass spectrum shown shaded in Fig. 17(b). Using the

TABLE VIII. Analysis results for the reaction $K^-p \to \Xi^-(1860)K^+$ in the final state $\Sigma^-\bar{K}^0K^+$. The top three entries are for the full sample of events. The bottom three entries are for the events remaining after the selection $\hat{K}^+ \cdot \hat{K}^- < 0.0$.

	Number of events	Percentage signal	Mass (MeV/c^2)	Width (MeV)	Cross section (μb)[a]	Number of resonant events
H_2	85	38 ± 12	1852 ± 14	63 ± 17	1.52 ± 0.55	32 ± 10
D_2	49	...	...	...	< 0.81	...
$H_2 + D_2$	134	27 ± 12	1854 ± 17	85 ± 35	1.30 ± 0.60	36 ± 16
H_2	59	47 ± 14	1855 ± 13	57 ± 15	1.37 ± 0.48	28 ± 8
D_2	29	...	...	...	< 1.14	...
$H_2 + D_2$	88	44 ± 13	1860 ± 14	72 ± 17	1.42 ± 0.47	39 ± 11

[a]Topological cross section uncorrected for neutral decays.

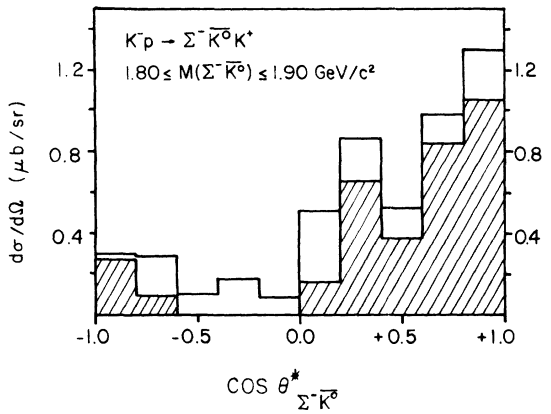

FIG. 16. Differential cross section for the $\Sigma^-\bar{K}^0$ system in the final state $\Sigma^-\bar{K}^0K^+$, obtained from the combined hydrogen and deuterium data, for events having $1.82 \leq M(\Sigma^-\bar{K}^0) \leq 1.90$ GeV/c^2. The shaded area results when a background, determined by events with $M(\Sigma^-\bar{K}^0) < 1.82$ GeV/c^2 and $M(\Sigma^-\bar{K}^0) > 1.90$ GeV/c^2, is subtracted.

cross section determined for the process $K^-p \rightarrow \Xi^-(1860)K^+$, $\Xi^-(1860) \rightarrow \Sigma^-\bar{K}^0$ in the final state $\Sigma^-\bar{K}^0K^+$, we would expect 20.5 ± 7.1 and 82 ± 28 Ξ^* events, respectively, in our Σ^0K^- mass distribution for Ξ^* isospins of $\frac{1}{2}$ or $\frac{3}{2}$. The mass interval $1.84 < M(\Sigma^0K^-) < 1.90$ GeV/c^2 yields an upper

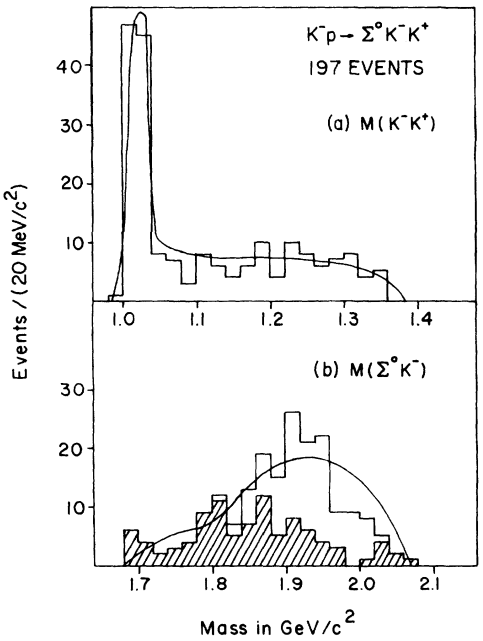

FIG. 17. The K^-K^+ and Σ^0K^- effective-mass distributions for the final state $\Sigma^0K^-K^+$. (a) $M(K^-K^+)$. (b) $M(\Sigma^0K^-)$. The shaded portion of (b) results from removal of events involving production of $\phi(1019)$ [$M(K^-K^+) < 1.05$ GeV/c^2]. The curves represent the fit obtained using the processes $K^-p \rightarrow \Sigma^0\phi(1019)$ and $K^-p \rightarrow \Sigma^0K^-K^+$.

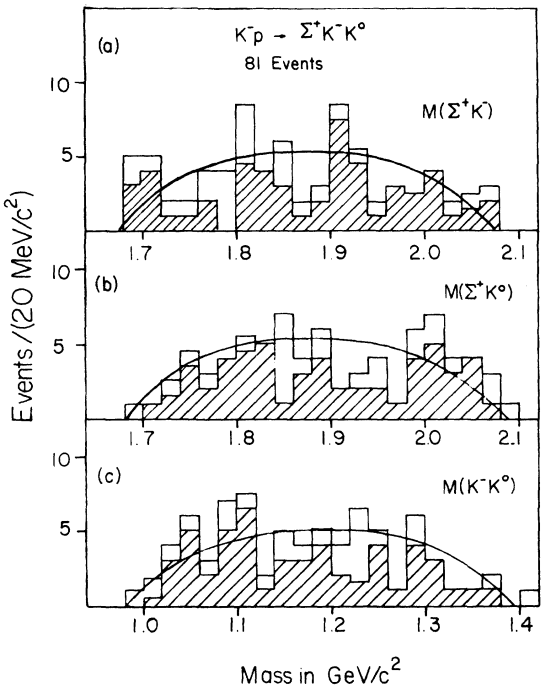

FIG. 18. Effective-mass distributions for the final state $\Sigma^+K^-K^0$, in the combined hydrogen and deuterium data. (a) $M(\Sigma^+K^-)$. (b) $M(\Sigma^+K^0)$. (c) $M(K^-K^0)$. The shaded area represents the hydrogen events. The curves are phase space normalized to the combined data.

limit of 13 resonant events at the 90% confidence level. This is only one standard deviation below the number expected if the effects observed in $\Sigma^-\bar{K}^0K^+$ are interpreted as production of an $I = \frac{1}{2}$ $\Xi^{*-}(1860)$.

I. $K^-p \rightarrow \Sigma^+K^-K^0$

The three mass distributions for the 81 events in the combined hydrogen and deuterium samples for this final state are shown in Fig. 18. The shaded portion is the contribution from the hydrogen data alone, and the solid curves represent phase space normalized to the complete sample. We observe no evidence for production of Ξ resonances in the $M(\Sigma^+K^-)$ spectrum, and place an upper limit of 1.1 μb at the 90% confidence level on the process $K^-p \rightarrow \Xi^{*0}K_1^0$, $\Xi^{*0} \rightarrow \Sigma^+K^-$ for a Ξ^* width less than 60 MeV.

J. $K^-p \rightarrow \Lambda\bar{K}\pi K$, $K^-p \rightarrow \Sigma\bar{K}\pi K$

The effective-mass distributions for the final states $Y\bar{K}\pi K$ have been investigated for evidence of Ξ^* production in the $Y\bar{K}$ and $Y\bar{K}\pi$ mass combinations. None has been observed. The Λ final states contain substantial amounts of $\Sigma(1385)$ production [$(45 \pm 18)\%$ of the 137 events]. The Σ final

states are dominated by production of $\phi(1019)$ ($\gtrsim 70\%$), $\Sigma(1385)$, and $\Lambda(1405)$. Approximately 50% of the sample involves quasi-two-body $Y^*\phi(1019)$ production.

VI. CONCLUSIONS

We have completed a search in 2.87-GeV/c K^-p interactions, at a sensitivity of 48 events/μb, for evidence of production of Ξ^* resonances decaying into $\Xi\pi$, $\Xi\pi\pi$, $Y\bar{K}$, and $Y\bar{K}\pi$. The data represent the combined results of a 30-events/μb experiment in hydrogen, and an 18-events/μb experiment in deuterium.

In Table IX we summarize the properties of the Ξ resonances which were found in these experiments. For each signal observed we give the fitted mass and width, as well as the percentage of resonant events in the specific final state. Wherever possible, we have also added the value of the production cross section times branching ratio in that particular final state. The parameter values quoted in Table IX supersede all previous Brandeis-Maryland-Syracuse-Tufts determinations of these quantities. They represent what we consider to be the most reliable values obtainable from our data, in accordance with the discussions in the text.

TABLE IX. Summary of results on Ξ^* production.

	Resonance	Final state	Mass (MeV/c^2)	Width (MeV)[a]	Percentage of total final state	$B \cdot \sigma$ (μb)[b]
(1)	$\Xi(1530)$	$(\Xi^-\pi^+)K^0$	1531[c]	13.9 ± 1.9	21.8 ± 1.8	14.2 ± 1.8
(2)		$(\Xi^-\pi^0)K^+$	1541 ± 6	43 ± 13	18.0 ± 3.8	5.5 ± 1.4
(3)		$(\Xi^0\pi^-)K^+$	1535	20 ± 10	10.1 ± 3.1	d
(4)	$\Xi(1630)$	$(\Xi^-\pi^+)K^0$	1624 ± 3	22.5	4.1 ± 1.4	2.6 ± 0.9
(5)		$(\Xi^-\pi^0)K^+$	...	...	< 3.8	< 1.2
(6)		$(\Xi^0\pi^-)K^+$	...	...	< 4.6	d
(7)	$\Xi(1820)$	$(\Xi^-\pi^+)K^0$	1797 ± 19	99 ± 57	9.9 ± 5.9	6.4 ± 3.8
(8)		$(\Xi^-\pi^0)K^+$	...	...	< 3.9	< 1.2
(9)		$(\Xi^0\pi^-)K^+$	...	...	< 4.9	d
(10)		$[\Xi(1530)\pi]K$	1829 ± 9	52 ± 34	(18.1 ± 3.5)[d]	e
(11)		$(\Sigma^-\bar{K}^0)K^+$	...	...	< 9.6	< 1.4
(12)		$(\Sigma^0K^-)K^+$	...	...	< 8.0	< 1.7
(13)		$(\Sigma^+K^-)K^0$	...	...	< 14.8	< 1.4
(14)		$(\Lambda\bar{K}^0)K^0$	...	...	< 1.9	< 1.4
(15)		$(\Lambda K^-)K^+$	1813 ± 4	26 ± 11	7.9 ± 2.3	6.0 ± 1.8
(16)	$\Xi(1860)$	$(\Xi^-\pi^+)K^0$	...	...	< 2.5	< 1.6
(17)		$(\Xi^-\pi^0)K^+$	...	...	< 4.6	< 1.4
(18)		$(\Xi^0\pi^-)K^+$	...	...	< 4.9	d
(19)		$(\Sigma^-\bar{K}^0)K^+$	1860 ± 14	72 ± 17	29.1 ± 8.2	4.3 ± 1.4
(20)		$(\Sigma^0K^-)K^+$	...	...	< 7.4	< 1.5
(21)		$(\Sigma^+K^-)\bar{K}^0$	...	...	< 12.2	< 1.1
(22)		$(\Lambda\bar{K}^0)K^0$	1870 ± 9	44 ± 11	6.1 ± 2.0	4.5 ± 1.4
(23)		$(\Lambda K^-)K^+$	...	...	< 5.1	< 3.9
(24)	$\Xi(1940)$	$(\Xi^-\pi^+)K^0$	1961 ± 18	159 ± 57	18.6 ± 5.6	12.0 ± 3.8
(25)		$(\Xi^-\pi^0)K^+$	...	...	< 5.2	< 1.6
(26)		$(\Xi^0\pi^-)K^+$	1936 ± 22	87 ± 26	14.8 ± 6.3	d
(27)		$[\Xi(1530)\pi]K$	1964 ± 10	60 ± 30	(15.0 ± 3.5)[e]	e
(28)		$(\Sigma^-\bar{K}^0)K^+$	...	...	< 8.3	< 1.2
(29)		$(\Sigma^0K^-)K^+$	...	...	< 5.0	< 1.0
(30)		$(\Sigma^+K^-)K^0$	...	...	< 11.9	< 1.1
(31)		$(\Lambda\bar{K}^0)K^0$	...	...	< 2.0	< 1.5
(32)		$(\Lambda K^-)K^+$	...	...	< 2.2	< 1.7

[a] The widths quoted here are empirical widths, not corrected for mass resolution. See Ref. 19 for an accurate determination of the $\Xi(1530)$ widths.

[b] Branching ratio times cross section. All cross sections are fully corrected. All upper limits are at the 90% confidence level.

[c] Underlined quantities were held fixed during the fits.

[d] Cross sections not calculated for this final state.

[e] The analysis of this final state was performed on a mixture of four different final-state topologies.

In addition, we have calculated upper limits[23] to resonance production cross sections for the final states in which no signal was visible at the expected mass. This information, often neglected, may be used in correlating signals in different channels and in deciding whether or not they may be attributed to the same resonant phenomenon. It can furthermore be used to obtain branching ratios or upper limits to branching ratios to be compared with various unitary symmetry models.

A few concluding comments on the various resonant mass regions are in order. In the following we shall denote by σ_0 and σ_- the production cross section of a given resonance in the two processes

$$\sigma_0 = \sigma(K^- p \to \Xi^{*0} K^0)$$

and

$$\sigma_- = \sigma(K^- p \to \Xi^{*-} K^+) .$$

A signal in the 1820-MeV/c^2 mass region has been seen in different experiments and final states,[3] and most recently clearly confirmed in the ΛK^- channel (Ref. 3, Gay *et al.*). We see a substantial signal in the ΛK^- and $\Xi(1530)\pi$ decay modes, and a weaker one for $\Xi\pi$ decay. From lines 14 and 15 in Table IX we find $\sigma_0 \leq (0.23 \pm 0.07)\sigma_-$ for $\Xi(1820) \to \Lambda\bar{K}$, while for $\Xi(1820) \to \Xi\pi$ lines 7 and 8 of the same table yield $\sigma_0 \geq (2.7 \pm 1.6)\sigma_-$. This apparent inconsistency may be understood in one of two ways: There is more than one $\Xi(1820)$, with $\Xi\pi$ and $\Lambda\bar{K}$ as dominant decay modes of the different resonances, or $\Xi(1820)$ does not in fact decay into $\Xi\pi$. In support of the latter hypothesis, the high-statistics experiment at 4.2 GeV/c of Gay *et al.*[3] does not observe the decay $\Xi^-(1820) \to (\Xi\pi)^-$.

Resonances in the 1940-MeV/c^2 mass region have also been observed by several authors.[3,21] We have observed signals in the $\Xi\pi$ and $\Xi(1530)\pi$ decay modes, with masses ranging from 1936 to 1964 MeV/c^2.

We observe possible signals in the $\Lambda\bar{K}^0$ and $\Sigma^-\bar{K}^0$ decay modes, in the 1860-MeV/c^2 mass region. No signals have been observed in this mass region in other experiments, with the exception of a very broad bump seen by Dauber *et al.*[3] in three-body $\Xi\pi K$ channels, and an excess of events having $1.80 \leq M(\Lambda K^-$ and $\Lambda K^0_{\text{forward}}) \leq 1.92$ GeV/c^2 observed in the final states $\Lambda K^- K^+$ and $\Lambda K^0 \bar{K}^0$ at 3.1–3.6 GeV/c by Ross *et al.*,[21] and interpreted there as two sharp peaks having masses of 1821 ± 5 MeV/c^2 and 1908 ± 4 MeV/c^2. If we try to identify our $\Lambda\bar{K}$ and $\Sigma\bar{K}$ signals as decay modes of the same resonance, then from lines 22 and 23 of Table IX we obtain $\sigma_0 \geq (1.15 \pm 0.36)\sigma_-$ for the $\Lambda\bar{K}$ decay mode, while for the $\Sigma\bar{K}$ decay mode lines 19 and 21 yield $\sigma_0 \leq (0.26 \pm 0.08)\sigma_-$. This appears to cast some doubt upon this interpretation.

The effect at about 1630 MeV/c^2 in the $\Xi\pi$ decay mode has been observed in the H_2 and, at a reduced level, the D_2 samples of this experiment, and also in other experiments at lower and higher beam momenta. On the other hand, significantly low upper limits to its production at other beam momenta have also been set and there appears to be no simple picture of the energy dependence of its production cross section. As a consequence, the effect needs further confirmation.

In conclusion we note that these two experiments have yielded some Ξ^* resonance production at the (5–10)-μb level, as well as upper limits at the (1–2)-μb level. It appears, therefore, that significant advances in Ξ spectroscopy will have to be made via experiments[24] with considerably greater sensitivity—i.e., in the (100 to 1000)-events/μb range.

ACKNOWLEDGMENTS

We wish to acknowledge the excellent work of the staff of the Brookhaven AGS and of the crew of the 31-in. bubble chamber. We are also deeply indebted to, and gratefully acknowledge, the diligent efforts of the scanners and measurers at the collaborating institutions.

---

†Work supported by the Energy Research and Development Administration.

‡Present address: George Washington University, Washington, D. C.

§Present address: Massachusetts Institute of Technology, Cambridge, Mass. 02138.

‖Present address: E. P. Division, CERN, 1211 Geneva 23, Switzerland.

¶Present address: Computer Sciences Corp., Silver Springs, Maryland 20910.

**Present address: Randall Physics Laboratory, Univ. of Michigan, Ann Arbor, Mich. 48104.

††Present address: Brookhaven National Laboratory, Upton, N. Y. 11973.

‡‡Present address: Physics Department, University of Cincinnati, Cincinnati, Ohio 45221; Work supported in part by NSF under Grant No. PHY72-04343A06.

§§Present address: University of Patras, Patras, Greece.

¶¶Present address: Digital Equipment Corp., Maynard, Mass. 01754.

[1] E. Briefel, S. A. Gourevitch, L. Kirsch, P. Schmidt, C. Y. Chang, R. Staab, G. B. Yodh, R. Fernow, P. Gauthier, G. Moneti, M. Goldberg, J. Canter, W. A. Mann, J. Schneps, J. Tompkins, and G. Wolsky, Phys. Rev. D 12, 1859 (1975).

[2]S. Apsell, N. Barash-Schmidt, L. Kirsch, P. Schmidt, C. Y. Chang, R. J. Hemingway, B. V. Khoury, A. R. Stottlemyer, H. Whiteside, G. B. Yodh, M. Goldberg, K. Jaeger, C. McCarthy, B. Meadows, G. C. Moneti, J. Bartley, R. M. Dowd, J. Schneps, and G. Wolsky, Phys. Rev. Lett. 23, 884 (1969); S. Apsell, N. Barash-Schmidt, L. Kirsch, P. Schmidt, C. Y. Chang, R. J. Hemingway, B. V. Khoury, A. R. Stottlemyer, H. Whiteside, G. B. Yodh, S. Glickman, M. Goldberg, K. Jaeger, C. McCarthy, S. Jacobs, B. Meadows, G. C. Moneti, J. Bartley, R. M. Dowd, J. Schneps, and G. Wolsky, *ibid.* 24, 777 (1970).

[3]G. A. Smith, J. S. Lindsey, J. J. Murray, J. Button-Shafer, A. Barbaro-Galtieri, O. I. Dahl, P. Eberhard, W. E. Humphrey, G. R. Kalbfleisch, R. R. Ross, F. T. Shively, and R. D. Tripp, Phys. Rev. Lett. 13, 61 (1964); G. A. Smith, J. S. Lindsey, J. Button-Shafer, and J. J. Murray, *ibid.* 14, 25 (1965); J. Badier, M. Demoulin, J. Goldberg, B. P. Gregory, C. Pelletier, A. Rouge, M. Ville, R. Barloutaud, A. Leveque, C. Louedec, J. Meyer, P. Schlein, A. Verglas, D. J. Holthuizen, W. Hoogland, and A. G. Tenner, Phys. Lett. 16, 171 (1965); J. Alitti, E. Flaminio, W. Metzger, D. Radojicic, R. R. Rau, N. P. Samios, I. Skillicorn, C. R. Richardson, D. Bassano, M. Goldberg, and J. Leitner, Phys. Rev. Lett. 21, 1119 (1968); J. Alitti, V. E. Barnes, E. Flaminio, W. Metzger, D. Radojicic, R. R. Rau, C. R. Richardson, N. P. Samios, D. Bassano, M. Goldberg, and J. Leitner, *ibid.* 22, 79 (1969); P. M. Dauber, J. B. Berge, J. R. Hubbard, D. W. Merrill, and R. A. Muller, Phys. Rev. 179, 1262 (1969); D. J. Crennell, U. Karshon, K. W. Lai, J. S. O'Neall, J. M. Scarr, and T. G. Schumann, Phys. Rev. D 1, 847 (1970); E. L. Goldwasser, and P. F. Schultz, *ibid.* 1, 1960 (1970); R. T. Ross, T. Buran, J. L. Lloyd, J. H. Mulvey, and D. Radojicic, Phys. Lett. 38B, 177 (1970); J. B. Gay, R. Armenteros, J. P. Berge, Ph. Gavillet, R. J. Hemingway, R. Blokzijl, G. G. G. Massaro, H. Voorthuis, P. M. Heinen, W. J. Metzger, D. J. Shotanus, H. G. Tiecke, J. J. M. Timmermans, and R. T. Van de Walle, *ibid.* 62B, 477 (1976).

[4]N. P. Samios, M. Goldberg, and B. T. Meadows, Rev. Mod. Phys. 46, 49 (1974).

[5]S. R. Borenstein, J. S. Danburg, G. R. Kalbfleisch, R. C. Strand, V. Vanderburg, J. W. Chapman, R. K. Kiang, and J. Lys, Phys. Rev. D 5, 1559 (1972); R. T. Ross *et al.*, Ref. 3.

[6]See, for example, R. H. Dalitz, in *Baryon Resonances—73*, proceedings of the Purdue Conference, edited by E. C. Fowler (Purdue Univ. Press, West Lafayette, Indiana, 1973), p. 393; R. Horgan, Nucl. Phys. B71, 514 (1974).

[7]Both beam K^- content and target purity were found to vary considerably over the six runs. During the last three runs the chamber fluid was contaminated with substantial amounts of H_2 and HD. This effectively reduces the neutron-target sensitivity (see Ref. 1) but does not affect proton sensitivity.

[8]To reduce the background from low-momentum $K^\pm$ decays, each event was required to have at least one visible decaying V^0.

[9]T. Hamada and I. Johnston, Nucl. Phys. 34, 382 (1962).

[10]We denote by the subscript 1 those decays of K^0, Λ, Ξ^0, Ξ^-, or Σ^0 in which the V^0 in the decay sequence decays via the charged mode ($\Lambda \to p\pi^-$, $K^0 \to \pi^-\pi^+$). A subscript 2 is used when the V^0 decay is not observed.

[11]E. Bracci, J. P. Droulez, E. Flamino, J. D. Hansen, and D. R. O. Morrison, CERN Report No. CERN/HERA 72-2, 1972 (unpublished).

[12]Uniformity in $X_{\pi\pi}$ for the reaction $K^-p \to \Lambda\pi^-\pi^+\pi^0$ is expected only if the sample does not contain significant numbers of events involving production of a $Y^{*0} \to \Lambda\pi^0$ with spin $>\frac{1}{2}$. We see no evidence for Y^* structure in $M(\Lambda\pi^0)$ for the ambiguous events under consideration.

[13]R. J. Hemingway and H. Whiteside, University of Maryland Technical Report No. 70-065, 1969 (unpublished); J. Tompkins, Tufts University Bubble Chamber Group Report No. 9-10, 1973 (unpublished).

[14]S. Derenzo and R. Hildebrand, Nucl. Instrum. Methods 69, 287 (1969).

[15]A. R. Stottlemyer, University of Maryland Technical Report No. 71-077, 1971 (unpublished).

[16]S. Jacobs, Ph. D. thesis, Syracuse University, 1972 (unpublished).

[17]A. de Bellefon, A. Berton, P. Billoir, J. M. Brunet, G. Tristam, J. Vrana, B. Baccari, G. Poulard, D. Revel, and B. Tallini, Nuovo Cimento 28A, 289 (1975).

[18]In all of our mass distributions we plot unweighted events (i.e., not corrected for geometric detection efficiency). No significant changes in any results occur when weighted events are used instead.

[19]The mass resolution has not been unfolded from the width determinations quoted in this paper. Accurate mass and true width determinations have been made for $\Xi^0(1530)$ [L. Kirsch, P. Schmidt, C. Y. Chang, R. Hemingway, B. V. Khoury, A. R. Stottlemyer, G. B. Yodh, S. Glickman, M. Goldberg, S. Jacobs, C. McCarthy, B. Meadows, G. C. Moneti, J. Sahouria, J. Canter, M. Govan, E. Katsoufis, J. Schneps, and G. Wolsky, Nucl. Phys. B40, 349 (1972)].

[20]Particle Data Group, Rev. Mod. Phys. 48, S1 (1976).

[21]R. T. Ross *et al.*, in *Baryon Resonances—73*, Ref. 6, p. 345.

[22]This procedure has been checked by using the same selections for the channel $K^-p \to \Lambda K^+K^-$, neglecting the charge of the kaons [R. Fernow, Ph. D. thesis, Syracuse University, 1973 (unpublished)]. The $M(\Lambda K^+)_{\text{forward}}$ distribution does retain most of the features of the $M(\Lambda K^-)$ spectrum, and similarly the $M(\Lambda K^+)_{\text{backward}}$ distribution reflects the distribution in $M(\Lambda K^+)$.

[23]The upper limits for production of a resonance seen in another channel were calculated in the following manner: A mass region having a width of 75 MeV/c^2, centered at the resonance mass, was selected. The number of events above a background curve, determined by phase space plus any identifiable resonances, was counted. (A negative number was replaced by zero.) These events were then considered to be the result of a 1.65-standard-deviation downward fluctuation from a larger number of "true" resonant events. This "true" number was then taken to represent the upper limit.

[24]For a discussion of present and future research activity see, for example, R. J. Hemingway, in *Proceedings of the Topical Conference on Baryon Resonances*, Oxford, 1976, edited by R. T. Ross and D. H. Saxon (Rutherford Laboratory, Chilton, Didcot, England), p. 355.